such conditions, the efficacy of ATR co-precipitation decreased to ~30% by purvalanol-A treatment (Fig. 2C). Immunoblotting with anti-phospho-S54-CDC6 antibodies revealed that purvalanol-A treatment indeed inhibited phosphorylation of 2HA-CDC6 by Cdk (Fig. 2C). In addition, we found that the interaction between ATR and 2HA-CDC6 EEE was not affected by purvalanol-A treatment (Fig. 2D), further supporting the notion that this drug affects ATR-CDC6 through inhibition of CDC6 phosphorylation by Cdk.

Taken together, these data led us to conclude that interaction of ATR with CDC6 is enhanced by CDC6 phosphorylation by Cdk. When cells are synchronized in early-mid G1 phase (6 hours after release from nocodazole arrest), CDC6 protein levels are remarkably decreased by APC/C^{Cdh1}-mediated ubiquitylation (data not shown) (Méndez and Stillman, 2000; Mailand and Diffley, 2005). As a result, in the present study, CDC6 immunoprecipitation with anti-CDC6 antibodies was remarkably reduced and ATR co-precipitation was undetectable in such cells (data not shown). Therefore, the observed co-precipitation between CDC6 and ATR in asynchronous cells might mainly represent interactions in S-phase cells. When cells were treated with 0.1 mM hydroxyurea (HU) for 4 hours, a condition we used to investigate CDC6 involvement in replication-checkpoint activation (see below), co-precipitation of ATR with CDC6 was not enhanced (Fig. 2E). Even with 2.5 mM HU treatment for 16 hours, the efficacy of the interaction was not changed (Fig. 2F).

CDC6 depletion by siRNA impairs ATR-dependent replication-checkpoint response and the defect is rescued by the CDC6 EEE mutant but not by CDC6 AAA

To determine whether CDC6 depletion by siRNA affects activation of a replication checkpoint in human cells, we designed siRNAs targeting 5′ untranslated regions of *CDC6* mRNA. Treatment with the *CDC6* siRNAs (6 nM) for 48 hours reduced the level of total CDC6 proteins to ~30% in HeLa cells compared with control-siRNA-treated cells (Fig. 3A). The effect was specific, because the level of MCM7 was not affected. Subcellular fractionation experiments showed that the level of chromatin-bound MCM7 proteins was decreased to ~70% by CDC6 depletion (Fig. 3A). Fluorescence-activated cell-sorting analysis showed that the cell-cycle distribution pattern is only slightly affected by CDC6 depletion (Fig. 3B). Cell growth was also largely unaffected (data not shown). Under the present experimental conditions in HeLa cells, CDC6 depletion did not induce spontaneous Chk1 phosphorylation (Fig. 3C), as reported previously (Lau et al., 2006; Kan et al., 2008). By

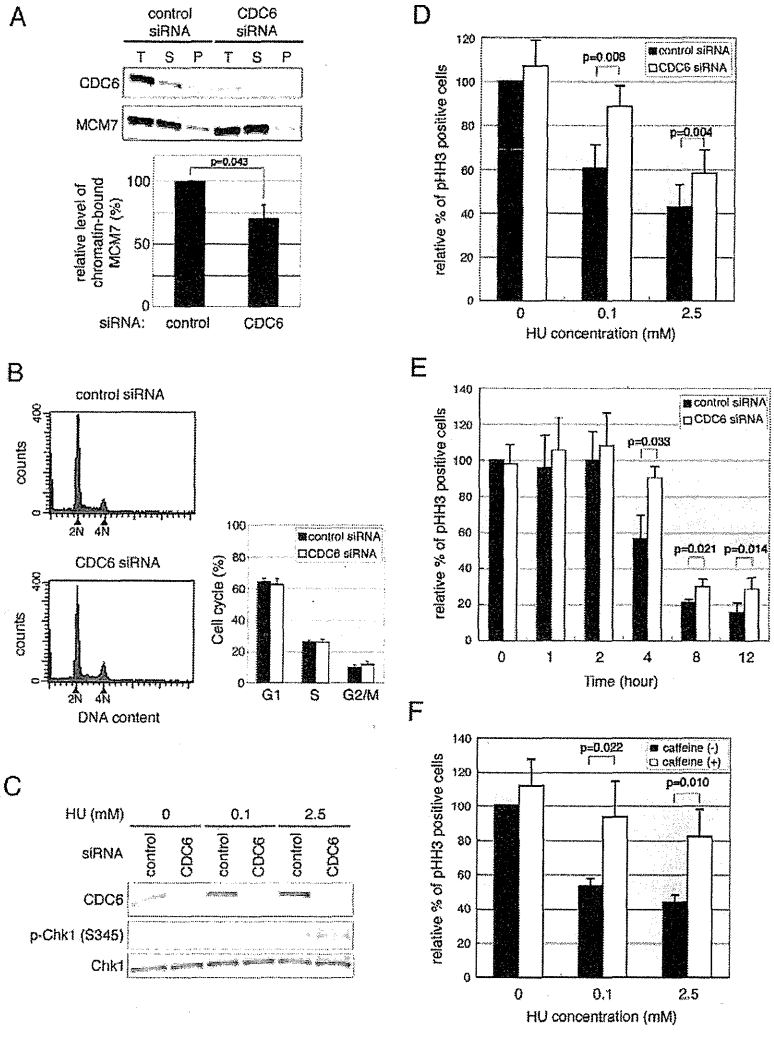

Fig. 3. CDC6 depletion by siRNA impairs the ATR-dependent replication-checkpoint response activated by modest replication stress. HeLa cells were transfected with siRNAs targeting 5′ untranslated regions of *CDC6* mRNA or with control siRNA for 48 hours. (**A**) Total cell extracts (T), Triton-X-100-extractable fractions (S), and nuclear chromatin and nuclear-matrix fractions (P) were then prepared and immunoblotted with anti-CDC6 or anti-MCM7 antibodies. The signal intensities of the chromatin-bound MCM7 proteins were quantified and normalized to those of total MCM7 to calculate the relative levels of chromatin-bound MCM7. The mean ± s.d. from three independent experiments are shown with the value for control-siRNA-treated cells set at 100 (lower panel). (**B**) Cell-cycle profiles were also analyzed by flow cytometry. The mean ± s.d. from three independent experiments are shown (right panel). (**C**) At 48 hours post-siRNA transfection, cells were treated with 2.5 mM or 0.1 mM HU, or left untreated, for a further 4 hours. Whole-cell lysates were then subjected to immunoblotting. p-Chk1, phospho-Chk1. (**D**) At 48 hours post-siRNA transfection, cells were treated with 2.5 mM or 0.1 mM HU, or left untreated, for a further 4 hours. Cells were then fixed and immunostained with anti-phospho-histone-H3 (pHH3) antibody followed by DAPI staining. The percentage of pHH3-positive cells was determined by microscopic observation of at least 3000 cells for each sample. The mean ± s.d. of five independent experiments are shown with control-siRNA-treated cells without HU set at 100%. (**E**) At 48 hours post-siRNA transfection, cells were treated with 0.1 mM HU for the times indicated. The percentage of pHH3-positive cells was then determined as in D. The mean ± s.d. of three independent experiments are shown with control-siRNA-treated cells at time 0 set at 100%. (**F**) At 48 hours after transfection with control siRNA, cells were incubated with 2.5 mM or 0.1 mM HU, or left untreated, for a further 4 hours. During the last 10 hours of incubation (i.e. from 6 hours before HU addition), 5 mM caffeine was also added, as indicated. The percentage of pHH3-positive cells was then determined as in D. The mean ± s.d. from four independent experiments are given with the value for control cells without drugs set at 100%.

contrast, it was reported that, when CDC6 is further depleted with more siRNAs (~100 nM), MCM loading is further reduced, leading to cell-cycle arrest around G1-S and/or cell death (Feng et al., 2003; Lau et al., 2009). Under such conditions, spontaneous Chk1 phosphorylation is observed.

We then investigated whether CDC6 depletion impairs ATR-mediated Chk1 phosphorylation induced by replication stress, such as polymerase inhibition. For these studies, CDC6-depleted or control-siRNA-treated HeLa cells were further treated with 2.5 mM HU for 4 hours and Chk1 phosphorylation was monitored with anti-phospho-S345-Chk1 antibodies (Zhao and Piwnica-Worms, 2001). As shown in Fig. 3C, robust phosphorylation of Chk1 was induced by 2.5 mM HU treatment and was not affected by CDC6 depletion, in agreement with previous findings that CDC6 depletion does not abolish Chk1 phosphorylation induced by treatment with 5 μg aphidicolin/ml in HeLa cells (Lau et al., 2006). Given the report that Chk1 phosphorylation induced by 1.5 mM HU treatment in HeLa cells is suppressed by 5 mM caffeine (Rodríguez-Bravo et al., 2006), an inhibitor for ATM and ATR, the above data and that of Lau et al. (Lau et al., 2006) suggest that CDC6 does not play a pivotal role in ATR activation by the stalled forks generated by 2.5 mM HU or 5 μg aphidicolin/ml.

However, Lau at el. also reported that CDC6-depleted HeLa cells (not treated with any drugs) prematurely enter mitosis despite the existence of actively replicating DNA (Lau et al., 2006). This suggested to us that CDC6 might be involved in replication-checkpoint activation elicited by modest replication stress. Extensive RPA-coated ssDNA is currently considered to be a crucial intermediate for ATR activation (Burrows and Elledge, 2008; Namiki and Zou, 2006; Zou and Elledge, 2003). We hypothesized that, although CDC6 is not necessarily required for activation of a replication checkpoint when there is sufficient RPA-coated ssDNAs, CDC6 might be required when replication stress is relatively modest. Therefore, because one crucial response elicited by replication-checkpoint activation involves a mitotic block (Kelly and Brown, 2000), we treated control-siRNA-transfected HeLa cells with various concentrations of HU for a relatively short period (i.e. 4 hours) and examined the effect of this on mitosis block by immunostaining the cells for phosphorylation of histone H3 at S10, a mitotic marker (data not shown). As expected, 2.5 mM HU treatment reduced the mitotic index to ~40% of that of untreated cells. Interestingly, we found that, even with 0.1 mM HU treatment, which reduces DNA synthesis by about 50% (Ge et al., 2007), HeLa cells were significantly inhibited in mitotic entry to a mitotic index of ~60%, suggesting that the replication checkpoint might be activated by low-dose HU treatment. We then tested whether CDC6 depletion affects the mitosis block. Although CDC6 depletion seemed to abrogate the mitotic block, at least partially, at all the HU concentrations tested, the effect was most prominent when cells were treated with 0.1 mM HU (data not shown). Therefore, we examined in more depth the influence of CDC6 depletion on mitotic block elicited by a 4-hour 0.1 mM HU treatment. As shown in Fig. 3D, CDC6 depletion increased the percentage of phospho-histone H3 (pHH3)-positive, mitotic cells by ~30% in cells treated with 0.1 mM HU, whereas it increased mitotic cells by only ~15% on treatment with 2.5 mM HU, suggesting that CDC6 plays a crucial role in replication-checkpoint activation by modest replication stress. Furthermore, we examined the effect of CDC6 depletion on mitotic block induced by 0.1 mM HU treatments at various time points (Fig. 3E). Longer incubation (8 and 12 hours) in the presence of 0.1 mM HU further decreased the amount of mitotic cells. Also under such conditions, CDC6 depletion resulted in a statistically significant increase in mitotic cells (Fig. 3E). However, the extent seemed to be limited compared with the 4-hour incubation.

Although the ATR-Chk1 pathway is a major component in replication-checkpoint activation (Guo et al., 2000; Hekmat-Nejad et al., 2000; Kumagai et al., 1998; Nghiem et al., 2001), several previous studies have indicated the existence of another pathway(s) to prevent premature mitotic entry upon replication stress (Brown and Baltimore, 2003; Rodríguez-Bravo et al., 2006; Zachos et al., 2003; Zachos et al., 2005). For example, it was previously shown that inhibition of mitotic entry in HeLa cells caused by 1.5 mM HU treatment for 25 hours is dependent on Chk1 and claspin but not on ATR and Rad17 (Rodríguez-Bravo et al., 2006). Therefore, we examined whether the replication-checkpoint response elicited by 0.1 mM (or 2.5 mM) HU for 4 hours depends on ATR by co-treating cells with HU and 5 mM caffeine. In order to compare the effect of caffeine with CDC6 depletion that occurs before the HU treatment (data not shown), we treated cells with 5 mM caffeine from 6 hours before the addition of HU. Caffeine was able to overcome the inhibition of mitotic entry induced by 0.1 mM HU (Fig. 3F), suggesting that activation of the replication checkpoint elicited by these experimental conditions depends on ATR (or possibly ATM). We found no detectable increase in Chk1 phosphorylation at S345 upon treatment with 0.1 mM HU for 4 hours (Fig. 3C). Therefore, even by modest replication stress in which Chk1 phosphorylation is not increased to an experimentally detectable level, an ATR-dependent replication checkpoint is activated and elicits a G2 arrest. This seems consistent with the fact that, in *Xenopus* egg extracts, ATR is required to prevent premature mitotic entry not only when replication is inhibited by exogenous stress but also during normal DNA replication, which might generate some internal replication stress (Hekmat-Nejad et al., 2000). Caffeine increased mitotic cells by ~40% also with 2.5 mM HU treatment (Fig. 3F) and the extent of recovery was higher than with CDC6 depletion (Fig. 3D), suggesting that CDC6 has rather a minor role in replication-checkpoint activation by strong replication stress.

To determine whether the abrogation of the checkpoint response is specifically due to the CDC6 depletion, we performed 'add-back' experiments. Because CDC6 interaction with ATR is enhanced by Cdk phosphorylation, we compared CDC6 EEE and CDC6 AAA. We established HeLa cell lines stably expressing 2HA-CDC6 AAA or EEE at similar levels (Fig. 4A). Analysis for subcellular localization of 2HA-CDC6 showed that almost all CDC6 AAA is bound to the chromatin and nuclear matrix, whereas most CDC6 EEE is in the soluble fraction with the rest bound to the chromatin and nuclear matrix (Sugimoto et al., 2009). These cells were then transfected with siRNAs targeting 5′ untranslated regions of *CDC6* mRNA, or control siRNA. Immunoblot analysis showed that exogenous 2HA-CDC6 protein levels were not affected by *CDC6* siRNA, whereas endogenous CDC6 decreased to ~30% (Fig. 4A).

Cells were further treated with 0.1 mM HU for 4 hours and mitotic indexes were determined. It has been reported that ionizing-radiation-induced DSBs activate the DNA-damage checkpoint, lead to Cdk downregulation and consequently induce APC/C^{Cdh1}-mediated CDC6 degradation (Duursma and Agami, 2005; Mailand and Diffley, 2005). CDC6 is also destabilized upon ultraviolet radiation (UV) and methyl-methane-sulfonate treatment through Huwe1-mediated ubiquitylation (Hall et al., 2007). We therefore examined the effects of HU treatment on CDC6 stability. The levels of endogenous CDC6 proteins in HeLa cells were not affected by

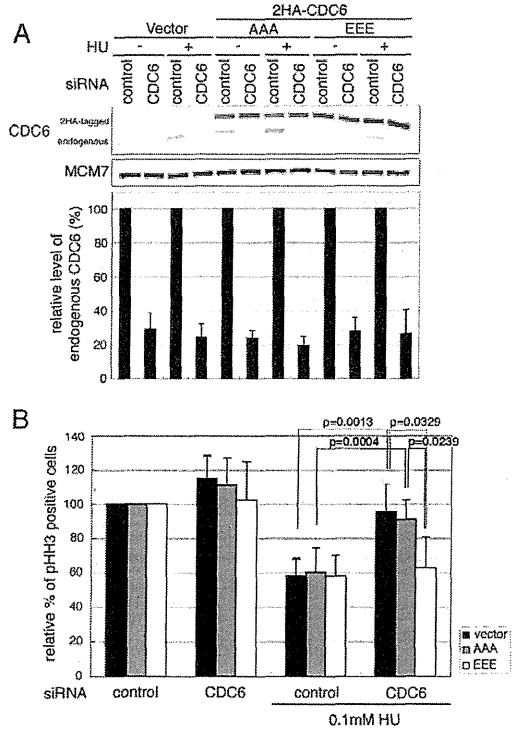

Fig. 4. The Cdk-phosphorylation-mimic CDC6 EEE mutant, but not the phospho-deficient AAA mutant, can rescue the defect in the replication-checkpoint response caused by CDC6 depletion. HeLa cells stably expressing the 2HA-CDC6 AAA or EEE mutant, or carrying a backbone vector, were established by retroviral infection. These cells were transfected with siRNAs targeting 5′ untranslated regions of *CDC6* mRNA or control siRNA for 48 hours, as described for Fig. 3. At 48 hours post-siRNA-transfection, cells were treated with 0.1 mM HU or left untreated for a further 4 hours. (**A**) Whole-cell lysates were immunoblotted. The signal intensities of the endogenous CDC6 bands were quantified and normalized to those of MCM7 to calculate CDC6 depletion efficiencies in each experiment. The mean ± s.d. from five independent experiments are shown with the value for control-siRNA-treated cells set at 100 (lower panel). (**B**) Cells were stained for pHH3 to determine the percentage of pHH3-positive cells, as described for Fig. 3. The mean ± s.d. of five independent experiments are shown with control-siRNA-treated cells without HU set at 100%.

either 0.1 mM or 2.5 mM HU treatment for 4 hours (Fig. 3C, Fig. 4A). Furthermore, the stability of transfected CDC6 AAA and CDC6 EEE mutant proteins was not differentially affected in response to 0.1 mM HU treatment for 4 hours (Fig. 4A). We also found that CDC6 is not destabilized by an 18-hour 2.5 mM HU treatment in normal human fibroblasts (data not shown). As reported, 10 or 25 J/m^2 UV irradiation resulted in CDC6 destabilization (data not shown). Therefore, replication-checkpoint activation by HU treatment might inhibit Cdk activity only to the extent that is insufficient for mitotic entry but enough for S-phase maintenance. It is generally considered that mitotic entry requires high Cdk activity.

In control HeLa cells with the backbone vector, CDC6 depletion abrogated the checkpoint response induced by 0.1 mM HU (Fig. 4B), as with parental HeLa cells. By contrast, despite *CDC6* siRNA treatment, mitotic entry was inhibited in HeLa cells with 2HA-CDC6 EEE (Fig. 4B), clearly demonstrating the CDC6 requirement for the ATR-dependent mitotic-block response. Interestingly, CDC6 AAA could not rescue the checkpoint defect (Fig. 4B). It was previously shown that *Xenopus* CDC6 mutants deficient in Cdk phosphorylation support normal replication with an efficiency comparable to that of wild type (Pelizon et al., 2000). We also found that 2HA-CDC6 AAA induces stronger re-replication than CDC6 EEE when transiently overexpressed with Cdt1 (Sugimoto et al., 2009). Therefore, CDC6 AAA might represent a novel mutant that specifically loses the ability to regulate ATR-dependent replication-checkpoint activation but retains the pre-RC-formation function. Taken together, these data strongly indicate that, in human cells, Cdk-phosphorylation-stimulated CDC6 interaction with ATR has a crucial role in replication-checkpoint activation elicited by modest replication stress.

The ATR-dependent checkpoint is also activated by UV irradiation. Thus, we tried to evaluate the role of CDC6 in UV-induced checkpoint activation. HeLa cells were irradiated with various doses of UV and, after 4 hours, examined for mitotic block and Chk1 phosphorylation. UV irradiation blocked mitotic entry in a dose-dependent manner, and Chk1 phosphorylation was also observed in a dose-dependent manner (data not shown). We then investigated the effects of CDC6 depletion on such UV-activated checkpoint responses. In contrast to HU treatment, CDC6-depleted HeLa cells were inhibited from mitotic entry in response to UV irradiation with comparable efficiency to control-siRNA-treated cells. Likewise, Chk1 phosphorylation was not affected by CDC6 depletion (data not shown). These data suggest that CDC6 might not be involved in UV-induced checkpoint responses. It is possible that intermediates for checkpoint activation and subsequent signaling pathways are different in some aspects between nucleotide-depletion-induced and UV-induced damage. For example, although 25 J/m^2 UV induced Chk1 phosphorylation at a comparable level to that by 2.5 mM HU treatment for 4 hours, the former inhibited mitotic entry more strongly (~100% versus ~60% inhibition) and destabilized CDC6 (data not shown). Whereas 0.1 mM HU treatment for 4 hours induced an ~40% mitotic block without detectable Chk1 phosphorylation (Fig. 3C-F), 5 J/m^2 UV inhibited mitosis by only ~20% despite obvious Chk1 phosphorylation (data not shown). Further in-depth studies will be required to dissect the molecular mechanisms.

Although our data indicate that CDC6-ATR interaction plays a role in the appropriate regulation of replication-checkpoint activation in human cells, it remains unclear how such interaction is involved in ATR activation. To address this issue, we first examined the possibility that CDC6 enhances ATR kinase activity as does TopBP1. Human ATR was immunopurified and the kinase activity was measured using PHAS1 as substrate. As previously reported (Hashimoto et al., 2006; Kumagai et al., 2006), addition of *Xenopus* Cut5 (XCut5; TopBP1) significantly increased the ATR kinase activity. Under these experimental conditions, GST-CDC6 EEE did not enhance the kinase activity. Addition of GST-CDC6 EEE to the reactions containing XCut5 also did not further increase the activity. Similar results were obtained with wild-type CDC6 (data not shown).

In fission yeast, Cdc18 stabilizes Rad3-Rad26 (ATR-ATRIP)-chromatin binding through physical interaction with Rad26 (Hermand and Nurse, 2007). Therefore, we examined whether stable ATR-chromatin binding is affected by CDC6 depletion in HeLa cells by immunodetecting the formation of bright nuclear ATR foci that might represent high-level accumulation of ATR at sites of DNA damage (Ball et al., 2005). The number of cells with

bright ATR foci increased slightly with 0.1 mM HU treatment for 4 hours and increased significantly with 2.5 mM HU treatment. However, the increase in number of ATR foci was not changed much by CDC6 depletion, suggesting that CDC6 is dispensable for stable high-level accumulation of ATR at sites at which DNA is extensively damaged. Also, clear colocalization of ATR foci with CDC6 was not observed (data not shown). Recently, it has been suggested that stable high-level retention of ATR at damaged sites is not necessarily required for some checkpoint responses (Ball et al., 2005). Therefore, it is possible that, although CDC6-ATR interaction does not mediate stable ATR retention at damaged sites, it does regulate dynamic association between ATR and small lesions. In this regard, it might be of interest that the human RPA complex binds to GST-CDC6 in pulldown assays, through the CDC6 region 1-180, which does not have a major role in CDC6-ATR interaction (data not shown).

XCDC6-XATR interaction is conserved in *Xenopus* and a human CDC6 fragment 180-220 that binds to XATR reduces XChk1 activation

In an in vitro DNA-replication system with *Xenopus* egg extracts, XCDC6 is required for XChk1 phosphorylation induced by polymerase inhibition (Oehlmann et al., 2004). Therefore, because XCDC6-XATR interaction might be conserved and play a crucial role in replication-checkpoint activation in *Xenopus* cells, we examined whether XCDC6 binds to XATR by pulldown assays. *Xenopus* egg extracts were mixed with GST or GST-XCDC6 and bound proteins were analyzed. XATR was found to bind to GST-XCDC6, but not to GST (Fig. 5A). In addition, XATR was found to co-immunoprecipitate with XCDC6 from egg extracts (Fig. 5B). Unfortunately, so far we could not determine whether the XCDC6-XATR interaction is affected by Cdk, mainly because of difficulty in specifically immunoprecipitating S-phase chromatin-bound XCDC6 with our anti-XCDC6 antibodies. Because CDC6-ATR interaction might be important for checkpoint activation, short CDC6 fragments that bind to XATR could inhibit XATR-dependent checkpoint responses by preventing physiological XCDC6-XATR interaction. Therefore, we repeated the pull-down experiments using *Xenopus* egg extracts and human CDC6 fragments fused to GST. As shown in Fig. 5C, XATR specifically bound to GST–human-CDC6. More importantly, XATR, similar to human ATR, bound to human CDC6 180-220 but not to CDC6 1-180 (Fig. 5C). The amino acid sequence of fragment 180-220 is conserved in XCDC6 (61% in identity). Taken together, these results indicate that CDC6-ATR interaction is a conserved feature in higher eukaryotic cells.

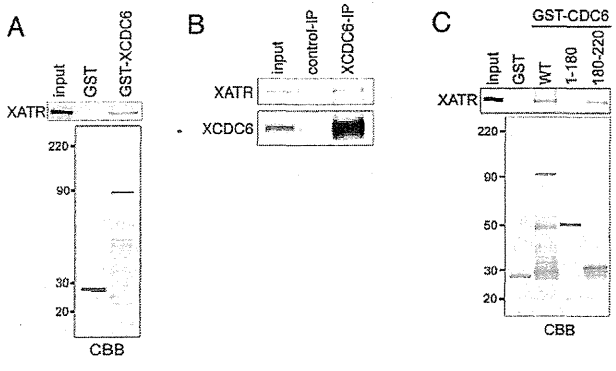

Fig. 5. CDC6-ATR interaction is conserved in *Xenopus* egg extracts. (**A**) GST–*Xenopus*-CDC6 (XCDC6) or GST was incubated with *Xenopus* egg extracts and bound proteins were analyzed by Coomassie Brilliant Blue (CBB) staining and immunoblotting with anti-XATR antibody. Fifty percent of the input was also loaded. (**B**) *Xenopus* egg extracts were immunoprecipitated with anti-XCDC6 antibodies or control rabbit IgG. The immunoprecipitates (IP) were subjected to immunoblotting with anti-XCDC6 and anti-XATR antibodies. A total of 1.6% of the input was also analyzed. (**C**) GST–human-CDC6 (WT; wild type), its truncated mutants (amino acids 1-180 and 180-220; see also Fig. 1) or GST was incubated with the egg extracts and bound proteins were analyzed by CBB staining and immunoblotting.

We first examined whether XCDC6 immunodepletion during S phase affects XATR recruitment onto chromatin in response to polymerase inhibition (Hekmat-Nejad et al., 2000). To address this, we adapted the nuclear transfer experiments (Fig. 6A). Licensed chromatin was isolated under high-salt conditions to remove chromatin-bound XCDC6 and then transferred to mock- or XCDC6-depleted extracts supplemented with aphidicolin to block DNA polymerases. After incubation for a further 45 minutes, chromatin was isolated and chromatin binding of XATR was analyzed by immunoblotting. Aphidicolin-induced recruitment of ATR to chromatin was significantly compromised by XCDC6 depletion (Fig. 6A). As previously reported (Oehlmann et al., 2004), DNA synthesis was not impaired by XCDC6 depletion from the second extracts (data not shown).

We found that the human CDC6 fragment 180-220 can partially prevent XATR binding to GST-XCDC6 when added to the egg extracts (Fig. 6B). Therefore, we tested whether this human CDC6 fragment can inhibit replication-checkpoint activation (Fig. 6C). For these studies, sperm chromatin was added to the egg extracts, which were then incubated for 15 minutes to allow pre-RC formation. Purified CDC6 fragment 180-220 with the SV40 T-antigen nuclear localization signal was then added to the reaction mixture at 10 ng/μl. The molar amount of CDC6 fragment was adjusted to 20-30 times higher than that of endogenous XCDC6 (Coleman et al., 1996). Aphidicolin (4 μg/ml) was also added to each reaction mixture and, after 45 minutes, isolated nuclei were immunoblotted with anti-phospho-S344-XChk1 antibody. Compared with control reactions with buffer alone or CDC6 fragment 1-180, which does not bind to XATR, phosphorylation of XChk1 induced by aphidicolin treatment was reduced by ~40% (Fig. 6D). We also investigated whether addition of CDC6 180-220 affects aphidicolin-induced recruitment of XATR to chromatin by immunoblotting analyses of chromatin fractions. Consistent with the reduction in XChk1 phosphorylation, aphidicolin-induced XATR chromatin recruitment was reduced by ~40% in the presence of CDC6 fragment 180-220 (Fig. 6E). In separate experiments, [^{32}P]-dCTP was added and the reactions were allowed to proceed for a further 45 minutes (without aphidicolin) after addition of the CDC6 fragments to monitor DNA replication. In all these reactions, DNA replication occurred at comparable levels (Fig. 6F), showing that the addition of CDC6 180-220 did not impair either pre-RC assembly or other replication reactions. Thus, human CDC6 fragment 180-220 specifically inhibits XATR-dependent XChk1 phosphorylation, probably through sequestrating XATR-XCDC6 interaction and XATR chromatin retention. Taken together, these data provide further support for our conclusion that CDC6 interacts with ATR and the CDC6-ATR interaction plays a crucial role in the regulation of replication-checkpoint activation in higher eukaryotic cells.

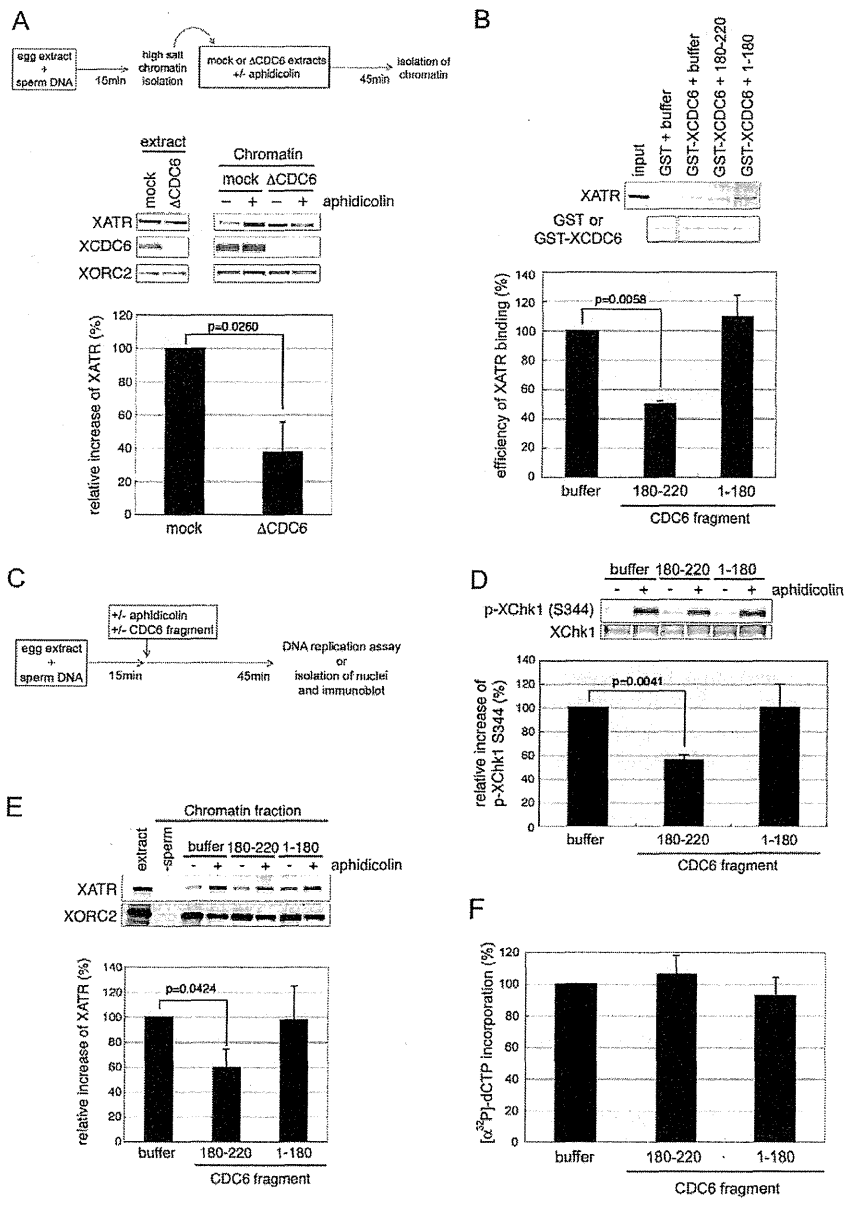

Fig. 6. CDC6-ATR interaction plays a role in activation of the replication checkpoint in *Xenopus* egg extracts. (**A**) XCDC6 immunodepletion during S phase reduces aphidicolin-induced XATR-chromatin binding. A schematic illustration of the experimental procedure is shown above. Sperm nuclei (4000/μl) were incubated in egg extracts for 15 minutes. Chromatin was then isolated under high-salt conditions and resuspended with mock- or XCDC6-depleted extracts. After a further 45-minute incubation, chromatin fractions were isolated and immunoblotted with the indicated antibodies. As indicated, aphidicolin (4 μg/ml) was added to the second extracts. The signal intensities of XATR bands induced by aphidicolin were normalized to those of XORC2 bands and plotted with the control reaction with mock-depleted extracts set at 100%. The mean ± s.d. from three independent experiments are shown. (**B-F**) Addition of human CDC6 amino acid fragment 180-220 after pre-RC assembly reduces XChk1 phosphorylation. (B) Human CDC6 fragments 180-220 or 1-180 with the SV40 T-antigen nuclear localization signal (but without GST) or buffer alone were added to *Xenopus* egg extracts. After incubation for 1.5 hours, these were then subjected to pulldown assays with GST-XCDC6, and bound proteins were analyzed by Coomassie Brilliant Blue (CBB) staining and immunoblotting. The signal intensities of the bands were quantitated and the efficiency of XATR binding to GST-XCDC6 was calculated as the intensity of the bound XATR relative to that of the pull-downed GST-XCDC6. The mean ± s.d. from three independent experiments are given with the control reaction with buffer alone set at 100% (lower panel). (C) Schematic of the experimental procedure for D, E and F. Sperm nuclei (2000/μl) were incubated in the egg extracts. After 15 minutes, human CDC6 fragments 180-220 or 1-180 with the SV40 T-antigen nuclear localization signal or buffer alone were added. (D,E) As indicated, aphidicolin (4 μg/ml) was also added to the reactions and, after a further 45-minute incubation, isolated nuclei (D) or chromatin (E) were immunoblotted with the indicated antibodies. The signal intensities of the phospho-Ser344 XChk1 (D) or XATR (E) bands induced by aphidicolin were quantified and normalized to those of whole XChk1 bands and XORC2 bands, respectively. The mean ± s.d. from three independent experiments are shown with the value for the control reaction with buffer alone set at 100% (each lower panel). (F) [^{32}P]-dCTP was added and, after a further 45-minute incubation, DNA replication was measured by [^{32}P] incorporation. The mean ± s.d. from three independent experiments are shown with the control reaction with buffer alone set at 100%.

Discussion

We have shown here that human CDC6 physically interacts with ATR in a Cdk-phosphorylation-stimulated manner (Figs 1, 2) and that CDC6 is required for the ATR-dependent replication-checkpoint response (i.e. inhibition of premature mitotic entry) activated by modest replication stress (Fig. 3). Interestingly, the defect in the checkpoint response caused by CDC6 depletion was rescued by the CDC6 EEE mutant mimicking Cdk phosphorylation, but not by the AAA mutant deficient in Cdk phosphorylation and ATR interaction (Fig. 4). Therefore, the CDC6 AAA mutant represents a mutant in which two functions of CDC6, replication licensing and replication-checkpoint regulation, are separated at the molecular level. In fission yeast, such mutant Cdc18 (CDC6) has not been identified yet. The region that we identified as an ATR-binding region on CDC6 does not include Cdk-phosphorylation sites (Fig. 1C). CDC6 is exported to the cytoplasm through Cdk phosphorylation but potential nuclear export signals on CDC6 are located at amino acids 462-488 (Delmolino et al., 2001), relatively distant from the Cdk-phosphorylation sites. However, it is conceivable that Cdk phosphorylation alters the high-order structure of CDC6 and thereby exposes the hidden nuclear export signals and ATR-binding region. In addition, the data reported here indicate that regulation of replication-checkpoint activation by CDC6-ATR interaction also occurs in *Xenopus* egg extracts: the XCDC6-XATR interaction was conserved (Fig. 5), and sequestration of the interaction by a human CDC6-derived peptide that binds to XATR reduced XATR chromatin recruitment and XChk1 phosphorylation induced by polymerase inhibition (Fig. 6).

These data, together with previously reported data in fission yeast (Hermand and Nurse, 2007), indicate that regulation of ATR-dependent replication-checkpoint activation through interaction between CDC6/CDC18 and ATR-ATRIP might be a conserved feature throughout eukaryotes. However, there are also differences among organisms. In the human cells studied here, this mechanism seems to play a crucial role for the replication checkpoint to be activated by modest replication stress, such as that elicited by 0.1 mM HU treatment (Fig. 3D,E, Fig. 4B), which reduces DNA synthesis by about half (Ge et al., 2007). Because CDC6 depletion alone (without additional replication perturbations) results in cells that prematurely enter mitosis with active DNA synthesis (Lau et al., 2006), the CDC6-ATR system might also operate against internal replication stress generated during the normal replication process. However, CDC6 in human cells seems dispensable for robust, ATR-dependent Chk1 phosphorylation induced by stronger replication stress, such as that induced by 2.5 mM HU treatment (Fig. 3C) (Lau et al., 2006). In addition, CDC6 is not required for ATR to accumulate at high levels in bright nuclear foci. CDC6 depletion somewhat affects ATR-dependent mitotic block activated by strong replication stress (i.e. 2.5 mM HU for 4 hours) but the relative contribution seems small (Fig. 3D,F).

A model that could reconcile these findings is depicted in Fig. 7. When replication stress is strong and, therefore, extensive RPA-coated ssDNA is generated, ATR-ATRIP molecules accumulate to high levels at the damaged sites through ATRIP-RPA interaction without the help of CDC6, forming bright ATR foci detectable by immunostaining, and robustly phosphorylate Chk1 (Fig. 7, left pathway). However, such high-level stable accumulation at damaged sites might be dispensable for ATR to be activated (Ball et al., 2005; Kim et al., 2005), although ATR foci formation could support some specific aspects of checkpoint responses. In other words, it is possible that only dynamic interaction between ATR and lesions is

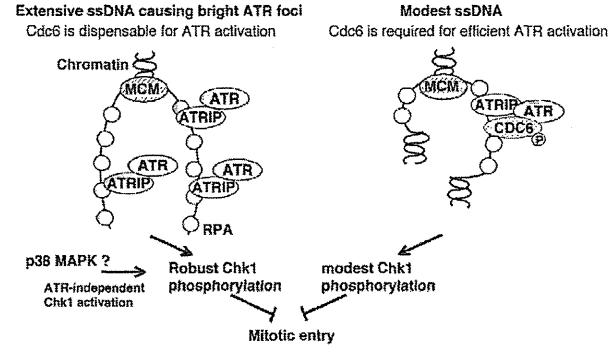

Fig. 7. Model for the role of human CDC6 in replication-checkpoint activation.

sufficient for ATR activation. In addition, in the presence of such extensive damage, another replication-checkpoint pathway(s) involving Chk1, but not ATR, could also be activated, leading to an ATR-independent (and thus caffeine-insensitive) block to mitosis (Rodríguez-Bravo et al., 2006). The p38 MAP kinase might be involved in such a pathway (Bulavin et al., 2001). Overall, CDC6 might have a minor role in checkpoint activation under such conditions.

However, even when cells are exposed to modest replication stress, ATR can be activated and delay mitotic entry despite low-level ATR foci formation and Chk1 phosphorylation (Fig. 3C,D). It is surprising that such low-level ATR activation can delay the cell cycle but, as in the *Xenopus* egg extract system, ATR is required to prevent premature mitotic entry not only when replication is inhibited by exogenous stress but also during normal DNA replication (Hekmat-Nejad et al., 2000). Presumably, fine regulatory control of the ATR-Chk1 pathway might function when cells encounter modest exogenous replication stress or endogenous replication stress. Under such circumstances, CDC6 and CDC6-ATR interaction might be required for ATR to elicit a mitotic block efficiently (Fig. 3D,E, Fig. 4B), presumably through regulating dynamic interaction between ATR and the damaged sites (Fig. 7, right pathway). Potential CDC6-RPA interactions could also play a role in this context. Extensive future studies will be required to clarify these points. Our present analyses of UV-damage-induced checkpoint responses found no indication of CDC6 involvement in these pathways. Although the details remain unclear, intermediates for checkpoint activation and subsequent signaling pathways might differ in some aspects between nucleotide-depletion-induced and UV-induced damage, as discussed above.

In contrast to human cells, in the *Xenopus* egg extract system, robust ATR-dependent Chk1 phosphorylation induced by 40 μM aphidicolin treatment seems dependent on XCDC6 (Oehlmann et al., 2004) and, as shown here, might be regulated by XCDC6-XATR interaction (Figs 5, 6). ATR chromatin recruitment induced by polymerase inhibition also depends on CDC6-ATR interaction in the *Xenopus* egg system (Fig. 6). The reason for the difference between the two systems, human cultured cells and *Xenopus* egg extracts, is not known at present. However, it should be emphasized that, even in the egg extract system, ORC-dependent, stable chromatin binding of XCDC6 is dispensable for XATR activation (Oehlmann et al., 2004), suggesting that the interactions between XCDC6 and the replication-checkpoint machinery are dynamic.

There is also a difference between human and fission yeast cells in terms of the CDC6-associated replication checkpoint. In yeast cells, Cdc18 (CDC6) is degraded during S phase depending on Cdk phosphorylation (Jallepalli et al., 1997; Jallepalli et al., 1998). Therefore, Cdc18 could not be involved in initial activation of the Rad3 (ATR)-dependent checkpoint. Attenuation of Cdk activity by the initial checkpoint activation then re-stabilizes Cdc18, which in turn interacts with Rad3-Rad26 (ATR-ATRIP) to sustain checkpoint activation (Hermand and Nurse, 2007). Therefore, these molecules seem to constitute a positive-feedback loop. However, in human cells, a significant part of CDC6 phosphorylated by Cdk remains in nuclei during S phase (Fujita et al., 1999) and CDC6 interaction with ATR is augmented by Cdk phosphorylation, as shown here (Fig. 2). Therefore, CDC6 might be involved in initial activation of an ATR-dependent checkpoint. When cells were treated with 0.1 mM HU for 4 hours, a condition under which we could definitely detect CDC6 involvement in replication-checkpoint activation, Cdk-phosphorylation-dependent CDC6 stabilization was not perturbed (Fig. 3C, Fig. 4A) and interaction of CDC6 with ATR was not affected (Fig. 2E). Therefore, ATR- and CDC6-dependent replication-checkpoint activation by modest replication stress might inhibit Cdk activity only to the extent that is insufficient for mitotic entry but enough for maintaining S-phase activity. If strong damage activates the replication checkpoint robustly and consequently inhibits Cdk activity markedly, then ATR-CDC6 interaction could be attenuated. However, under such conditions, CDC6 might be dispensable for checkpoint activation.

Materials and Methods

Cells

HeLa and 293T cells were grown in Dulbecco's modified Eagle's medium with 8% fetal calf serum. The chemicals used were: MG132 (Calbiochem), purvalanol A (Calbiochem), hydroxyurea (Sigma), caffeine (Nacalai) and aphidicolin (Sigma).

Expression of recombinant proteins and pulldown assay

GST-fusion proteins were bacterially produced and purified. GST pulldown assays were performed as described previously (Sugimoto et al., 2008), with 200 μg GST-fusion proteins per 2 ml extract from 1×10^8 cells. For pulldown assays with *Xenopus* egg extracts, 20 μl extracts were 40-fold diluted and then 6 μg GST-fusion proteins were added to the samples. Binding reactions for GST-fusion proteins were performed for 5 hours at 4°C. Human CDC6 fragments added to the *Xenopus* egg extracts were purified from the GST-fusion proteins by digestion with PreScission Protease (GE Healthcare).

Transfection and infection

293T cells were transfected as described previously (Sugimoto et al., 2008). HeLa cells were infected with retroviruses expressing the 2HA-CDC6 AAA mutant or EEE mutant, or with control retroviruses and selected with puromycin (0.5 μg/ml) as described (Sugimoto et al., 2008).

Immunoprecipitation and immunoblotting

Cells were extracted with modified CSK buffer containing 500 mM NaCl, 0.1% Triton X-100, 1 mM dithiothreitol (DTT) and multiple protease inhibitors (Sugimoto et al., 2008). Aliquots of the extracts were then immunoprecipitated with the indicated antibodies and protein-G–Sepharose beads (Amersham Bioscience). The beads were washed three times with NET gel buffer (Sugimoto et al., 2008). Immunoblotting and quantitation of the band signals were performed as described previously (Sugimoto et al., 2008).

siRNA experiments

siRNA oligonucleotides (IDT) were synthesized with the following sequences (sense strand): CDC6-1 (5′-AGACUAUAACUCUACAGAUUGUGdAdA-3′), CDC6-3 (5′-GGAGGACACUGGUUAAAGAAUUUdAdT-3′) and control scrambled (5′-CUUCCUCUCUUUCUCUCCCUUGUdGdA-3′). HeLa cells (4×10^4 cells per well in 12-well plates) were transfected with a 1:1 mixture of CDC6-1 and CDC6-3 or control siRNA duplexes (total 12 pmol; 6 nM) using HiPerFect transfection Reagent (Qiagen).

Immunostaining for phospho-histone H3

HeLa cells were washed, fixed with 3.7% formaldehyde, extracted with modified CSK buffer containing 0.1% Triton X-100, and then incubated overnight at 4°C with mouse anti-Ser10-phosphorylated histone H3 antibody. The samples were further incubated for 2 hours with Alexa-Fluor-594-conjugated goat anti-mouse IgG antibody (Molecular Probes), counterstained with DAPI and analyzed with a Leica FW4000 microscope.

Experiments with *Xenopus* egg extracts

Preparation of interphase egg extracts and de-membranated sperm nuclei, and the in vitro DNA-replication experiments were performed as described previously (Yoshida et al., 2005). Chromatin transfer experiments were performed as described previously (Hashimoto et al., 2006). Briefly, licensed sperm chromatin obtained after 15 minutes pre-incubation were diluted with ten volumes of EB buffer containing 0.1 mM NaCl and 2 mM DTT (Yoshida et al., 2005) and then centrifuged through a 20% sucrose layer at 10,000 ***g*** at 4°C for 5 minutes. The pellets were washed with EB containing 2 mM DTT and resuspended in second egg extracts. Immunodepletion of XCDC6 was carried out using 75 μl of anti-XCDC6 antisera for 100 μl egg extract (Yoshida et al., 2005). Nuclear and chromatin fractions were prepared as described previously (Kumagai et al., 1998; Yoshida et al., 2005). For immunoprecipitation, extracts were diluted with EB and then immunoprecipitated with the indicated antibodies and protein-G–Dynabeads (Invitrogen). The beads were washed three times with EB buffer containing 130 mM KCl.

Plasmids

For bacterial expression of GST-CDC6, pGEX6P-1-CDC6 was constructed by inserting human *CDC6* cDNA into pGEX6P-1 (GE Healthcare). *CDC6* truncated fragments were amplified by PCR using combinations of the following primers: 5′-1 primer, 5′-CGGGATCCGCTGTCGTCATGCCTCAAACCCG-3′; 5′-89 primer, 5′-CGGGATCCCATACACTTAAGGGACGAAGATTGG-3′; 5′-180 primer, 5′-CGGGATCCGATGTCATCAGGAATTTCTTGAGGG-3′; 3′-180 primer, 5′-TTA-AGCGGCCGCCTAATCCATCTCCCTTTCCCTGGC-3′; 3′-220 primer, 5′-TTAA-GCGGCCGCCTACTTGAGGTCTTGCAGAATCCG-3′; and 3′-268 primer, 5′-TTAAGCGGCCGCCTATTCCAATTTCCTCATCATGTCCTTC-3′. These PCR products were digested by *Bam*HI and *Not*I and subcloned into pGEX6P-1. For construction of fused SV40 T-antigen nuclear localization signal (NLS)-CDC6 fragments, an oligonucleotide containing the SV40 T-antigen NLS/*Bam*HI site/*Hin*dIII site sequence (5′-GATCGCCTAAAAAGAAGCGTAAAGTCGGATCCAAGCTTG-3′) and its complementary oligonucleotide were synthesized, annealed, inserted into the pGEX6P-1 *Bam*HI-*Eco*RI site, and CDC6 fragments were then introduced into the *Bam*HI-*Not*I site. pGEX6P-2-XCDC6 was provided by Haruhiko Takisawa (Osaka University, Osaka, Japan). Retrovirus vector pQCXIP-2HA-CDC6 was constructed by inserting *CDC6* cDNA tagged with tandem HA at its N-terminus into pQCXIP with a puromycin-resistance gene (Clontech). The cDNAs encoding Cdk-phosphorylation-deficient CDC6 AAA (Ser54, Ser74 and Ser106 were replaced with alanines) and phosphorylation-mimic EEE (Ser54, Ser74 and Ser106 were replaced with glutamates) mutants were gifts from Wei Jiang (Burnham Institute for Medical Research, La Jolla, CA). pBJ5.1-FLAG-ATR (Cliby et al., 1998) was kindly provided by Karlene Cimprich (Stanford University, Palo Alto, CA).

Antibodies

Preparation of antibodies against human CDC6, human MCM7, *Xenopus* ATR and *Xenopus* Chk1 were described previously (Hashimoto et al., 2006; Sugimoto et al., 2008). Antibodies against human Rad9, Hus1 and Rad1 were provided by Toshiki Tsurimoto (Kyushu University, Fukuoka, Japan). Other antibodies were purchased as follows: ATM (2C1, GeneTex), ATR (sc1887, Santa Cruz Biotechnology), ATRIP (number 2737, Cell Signaling), Cdh1 (c7855, Sigma), Chk1 (06-965, Upstate), Chk2 (05-649, Upstate), Claspin (ab3720, Abcam), cyclin A (sc596, Santa Cruz Biotechnology), Mre11 (611366, BD Bioscience), FLAG-M2 (F3165, Sigma Aldrich), Nbs1 (611870, BD Bioscience), Ser10-phosphorylated histone H3 (number 9706, Cell Signaling), Ser345-phosphorylated-Chk1 (number 2341 or 2348, Cell Signaling), Ser54-phosphorylated-CDC6 (sc12920R, Santa Cruz Biotechnology) and TopBP1 (ab2402, Abcam).

Statistical analysis

Statistical analysis was performed by a two-tailed Student's *t*-test to validate the data. *P*-values of <0.05 were considered statistically significant.

We thank Haruhiko Takisawa, Toshiki Tsurimoto, Wei Jiang, Koji Ode and Karlene Cimprich for Materials. We are also grateful to Satoko Yoshida, Chie Ogawa and Akiko Noguchi for assistance. This work was supported in part by a Grant to M.F. from the Ministry of Education, Culture, Sports, Science and Technology of Japan.

References

Ball, H. L., Myers, J. S. and Cortez, D. (2005). ATRIP binding to replication protein A-single-stranded DNA promotes ATR-ATRIP localization but is dispensable for Chk1 phosphorylation. *Mol. Biol. Cell* **16**, 2372-2381.

Bartek, J. and Lukas, J. (2003). Chk1 and Chk2 kinases in checkpoint control and cancer. *Cancer Cell* **3**, 421-429.

Bell, S. P. and Dutta, A. (2002). DNA replication in eukaryotic cells. *Annu. Rev. Biochem.* **71**, 333-374.

Brown, E. J. and Baltimore, D. (2003). Essential and dispensable roles of ATR in cell cycle arrest and genome maintenance. *Genes Dev.* **17**, 615-628.

Bulavin, D. V., Higashimoto, Y., Popoff, I. J., Gaarde, W. A., Basrur, V., Potapova, O., Appella, E. and Fornace, A. J., Jr (2001). Initiation of a G2/M checkpoint after ultraviolet radiation requires p38 kinase. *Nature* **411**, 102-107.

Burrows, A. E. and Elledge, S. J. (2008). How ATR turns on: TopBP1 goes on ATRIP with ATR. *Genes Dev.* **22**, 1416-1421.

Clay-Farrace, L., Pelizon, C., Santamaria, D., Pines, J. and Laskey, R. A. (2003). Human replication protein Cdc6 prevents mitosis through a checkpoint mechanism that implicates Chk1. *EMBO J.* **22**, 704-712.

Coleman, T. R., Carpenter, P. B. and Dunphy, W. G. (1996). The Xenopus Cdc6 protein is essential for the initiation of a single round of DNA replication in cell-free extracts. *Cell* **87**, 53-63.

Cortez, D., Guntuku, S., Qin, J. and Elledge, S. J. (2001). ATR and ATRIP: partners in checkpoint signaling. *Science* **294**, 1713-1716.

Cliby, W. A., Roberts, C. J., Cimprich, K. A., Stringer, C. M., Lamb, J. R., Schreiber, S. L. and Friend, S. H. (1998). Overexpression of a kinase-inactive ATR protein causes sensitivity to DNA-damaging agents and defects in cell cycle checkpoints. *EMBO J.* **17**, 159-169.

Delmolino, L. M., Saha, P. and Dutta, A. (2001). Multiple mechanisms regulate subcellular localization of human CDC6. *J. Biol. Chem.* **276**, 26947-26954.

Diffley, J. F. X. (2004). Regulation of early events in chromosome replication. *Curr. Biol.* **14**, R778-R786.

Drury, L. S., Perkins, G. and Diffley, J. F. X. (1997). The Cdc4/34/53 pathway targets Cdc6p for proteolysis in budding yeast. *EMBO J.* **16**, 5966-5976.

Duursma, A. and Agami, R. (2005). p53-dependent regulation of Cdc6 protein stability controls cellular proliferation. *Mol. Cell. Biol.* **25**, 6937-6947.

Feng, D., Tu, Z., Wu, W. and Liang, C. (2003). Inhibiting the expression of DNA replication-initiation proteins induces apoptosis in human cancer cells. *Cancer Res.* **63**, 7356-7364.

Fujita, M. (2006). Cdt1 revisited: complex and tight regulation during the cell cycle and consequences of deregulation in mammalian cells. *Cell Div.* **1**, 22.

Fujita, M., Yamada, C., Goto, H., Yokoyama, N., Kuzushima, K., Inagaki, M. and Tsurumi, T. (1999). Cell cycle regulation of human CDC6 protein. Intracellular localization, interaction with the human MCM complex, and CDC2 kinase-mediated hyperphosphorylation. *J. Biol. Chem.* **274**, 25927-25932.

Ge, X. Q., Jackson, D. A. and Blow, J. J. (2007). Dormant origins licensed by excess Mcm2-7 are required for human cells to survive replicative stress. *Genes Dev.* **21**, 3331-3341.

Gray, N. S., Wodicka, L., Thunnissen, A. M., Norman, T. C., Kwon, S., Espinoza, F. H., Morgan, D. O., Barnes, G., LeClerc, S., Meijer, L. et al. (1998). Exploiting chemical libraries, structure, and genomics in the search for kinase inhibitors. *Science* **281**, 533-538.

Guo, Z., Kumagai, A., Wang, S. X. and Dunphy, W. G. (2000). Requirement for Atr in phosphorylation of Chk1 and cell cycle regulation in response to DNA replication blocks and UV-damaged DNA in *Xenopus* egg extracts. *Genes Dev.* **14**, 2745-2756.

Hall, J. R., Kow, E., Nevis, K. R., Lu, C. K., Luce, K. S., Zhong, Q. and Cook, J. G. (2007). Cdc6 stability is regulated by the Huwe1 ubiquitin ligase after DNA damage. *Mol. Biol. Cell* **18**, 3340-3350.

Hashimoto, Y., Tsujimura, T., Sugino, A. and Takisawa, H. (2006). The phosphorylated C-terminal domain of *Xenopus* Cut5 directly mediates ATR-dependent activation of Chk1. *Genes Cells* **11**, 993-1007.

Hekmat-Nejad, M., You, Z., Yee, M. C., Newport, J. W. and Cimprich, K. A. (2000). *Xenopus* ATR is a replication-dependent chromatin-binding protein required for the DNA replication checkpoint. *Curr. Biol.* **10**, 1565-1573.

Herbig, U., Marlar, C. A. and Fanning, E. (1999). The Cdc6 nucleotide-binding site regulates its activity in DNA replication in human cells. *Mol. Biol. Cell* **10**, 2631-2645.

Hermand, D. and Nurse, P. (2007). Cdc18 enforces long-term maintenance of the S phase checkpoint by anchoring the Rad3-Rad26 complex to chromatin. *Mol. Cell* **26**, 553-563.

Jallepalli, P. V., Brown, G. W., Muzi-Falconi, M., Tien, D. and Kelly, T. J. (1997). Regulation of the replication initiator protein $p65^{cdc18}$ by CDK phosphorylation. *Genes Dev.* **11**, 2767-2779.

Jallepalli, P. V., Tien, D. and Kelly, T. J. (1998). sud1(+) targets cyclin-dependent kinase-phosphorylated Cdc18 and Rum1 proteins for degradation and stops unwanted diploidization in fission yeast. *Proc. Natl. Acad. Sci. USA* **95**, 8159-8164.

Jiang, W., Wells, N. J. and Hunter, T. (1999). Multistep regulation of DNA replication by Cdk phosphorylation of HsCdc6. *Proc. Natl. Acad. Sci. USA* **96**, 6193-6198.

Kan, Q., Jinno, S., Kobayashi, K., Yamamoto, H. and Okayama, H. (2008).Cdc6 determines utilization of $p21^{WAF1/CIP1}$-dependent damage checkpoint in S phase cells. *J. Biol. Chem.* **283**, 17864-17872.

Kastan, M. B. and Bartek, J. (2004). Cell-cycle checkpoints and cancer. *Nature* **432**, 316-323.

Kelly, T. J. and Brown, G. W. (2000). Regulation of chromosome replication. *Annu. Rev. Biochem.* **69**, 829-880.

Kim, S. M., Kumagai, A., Lee, J. and Dunphy, W. G. (2005). Phosphorylation of Chk1 by ATM- and Rad3-related (ATR) in *Xenopus* egg extracts requires binding of ATRIP to ATR but not the stable DNA-binding or coiled-coil domains of ATRIP. *J. Biol. Chem.* **280**, 38355-38364.

Kominami, K. and Toda, T. (1997). Fission yeast WD-repeat protein pop1 regulates genome ploidy through ubiquitin-proteasome-mediated degradation of the CDK inhibitor Rum1 and the S-phase initiator Cdc18. *Genes Dev.* **11**, 1548-1560.

Kumagai, A., Guo, Z., Emami, K. H., Wang, S. X. and Dunphy, W. G. (1998). The *Xenopus* Chk1 protein kinase mediates a caffeine-sensitive pathway of checkpoint control in cell-free extracts. *J. Cell Biol.* **142**, 1559-1569.

Kumagai, A., Lee, J., Yoo, H. Y. and Dunphy, W. G. (2006). TopBP1 activates the ATR-ATRIP complex. *Cell* **124**, 943-955.

Lau, E., Zhu, C., Abraham, R. T. and Jiang, W. (2006). The functional role of Cdc6 in S-G2/M in mammalian cells. *EMBO Rep.* **7**, 425-430.

Lau, E., Chiang, G. G., Abraham, R. T. and Jiang, W. (2009). Divergent S phase checkpoint activation arising from prereplicative complex deficiency controls cell survival. *Mol. Biol. Cell* **20**, 3953-3964.

Lee, J., Kumagai, A. and Dunphy, W. G. (2003). Claspin, a Chk1-regulatory protein. monitors DNA replication on chromatin independently of RPA, ATR, and Rad17. *Mol. Cell* **11**, 329-340.

Lee, J. H. and Paull, T. T. (2005). ATM activation by DNA double-strand breaks through the Mre11-Rad50-Nbs1 complex. *Science* **308**, 551-554.

Mailand, N. and Diffley, J. F. X. (2005). CDKs promote DNA replication origin licensing in human cells by protecting Cdc6 from APC/C-dependent proteolysis. *Cell* **122**, 915-926.

Méndez, J. and Stillman, B. (2000). Chromatin association of human origin recognition complex, Cdc6, and minichromosome maintenance proteins during the cell cycle: Assembly of prereplication complexes in late mitosis. *Mol. Cell. Biol.* **20**, 8602-8612.

Méndez, J., Zou-Yang, X. H., Kim, S. Y., Hidaka, M., Tansey, W. P. and Stillman, B. (2002). Human origin recognition complex large subunit is degraded by ubiquitin-mediated proteolysis after initiation of DNA replication. *Mol. Cell* **9**, 481-491.

Mordes, D. A., Glick, G. G., Zhao, R. and Cortez, D. (2008). TopBP1 activates ATR through ATRIP and a PIKK regulatory domain. *Genes Dev.* **22**, 1478-1489.

Namiki, Y. and Zou, L. (2006). ATRIP associates with replication protein A-coated ssDNA through multiple interactions. *Proc. Natl. Acad. Sci. USA* **103**, 580-585.

Nghiem, P., Park, P. K., Kim, Y., Vaziri, C. and Schreiber, S. L. (2001). ATR inhibition selectively sensitizes G1 checkpoint-deficient cells to lethal premature chromatin condensation. *Proc. Natl. Acad. Sci. USA* **98**, 9092-9097.

Nyberg, K. A., Michelson, R. J., Putnam, C. W. and Weinert, T. A. (2002). Toward maintaining the genome: DNA damage and replication checkpoints. *Annu. Rev. Genet.* **36**, 617-656.

Oehlmann, M., Score, A. J. and Blow, J. J. (2004). The role of Cdc6 in ensuring complete genome licensing and S phase checkpoint activation. *J. Cell Biol.* **165**, 181-190.

Pelizon, C., Madine, M. A., Romanowski, P. and Laskey, R. A. (2000). Unphosphorylatable mutants of Cdc6 disrupts its nuclear export but still support DNA replication once per cell cycle. *Genes Dev.* **14**, 2526-2533.

Petersen, B. O., Lukas, J., Sørensen, C. S., Bartek, J. and Helin, K. (1999). Phosphorylation of mammalian CDC6 by cyclin A/CDK2 regulates its subcellular localization. *EMBO J.* **18**, 396-410.

Rodríguez-Bravo, V., Guaita-Esteruelas, S., Florensa, R., Bachs, O. and Agell, N. (2006). Chk1- and claspin-dependent but ATR/ATM- and Rad17-independent DNA replication checkpoint response in HeLa cells. *Cancer Res.* **66**, 8672-8679.

Saha, P., Chen, J., Thome, K. C., Lawlis, S. J., Hou, Z. H., Hendricks, M., Parvin, J. D. and Dutta, A. (1998). Human CDC6/Cdc18 associates with Orc1 and cyclin-cdk and is selectively eliminated from the nucleus at the onset of S phase. *Mol. Cell. Biol.* **18**, 2758-2767.

Sugimoto, N., Kitabayashi, I., Osano, S., Tatsumi, Y., Yugawa, T., Narisawa-Saito, M., Matsukage, A., Kiyono, T. and Fujita, M. (2008). Identification of novel human Cdt1-binding proteins by a proteomics approach: proteolytic regulation by APC/C^{Cdh1}. *Mol. Biol. Cell* **19**, 1007-1021.

Sugimoto, N., Yoshida, K., Tatsumi, Y., Yugawa, T., Narisawa-Saito, M., Waga, S., Kiyono, T. and Fujita, M. (2009). Redundant and differential regulation of multiple licensing factors ensures prevention of re-replication in normal human cells. *J. Cell Sci.* **122**,1184-1191.

Villerbu, N., Gaben, A. M., Redeuilh, G. and Mester, J. (2002). Cellular effects of purvalanol A: a specific inhibitor of cyclin-dependent kinase activities. *Int. J. Cancer* **97**, 761-769.

Williams, R. S., Shohet, R. V. and Stillman, B. (1997). A human protein related to yeast Cdc6p. *Proc. Natl. Acad. Sci. USA* **94**, 142-147.

Yoshida, K., Takisawa, H. and Kubota, Y. (2005). Intrinsic nuclear import activity of geminin is essential to prevent re-initiation of DNA replication in Xenopus eggs. *Genes Cells* **10**, 63-73.

Zachos, G., Rainey, M. D. and Gillespie, D. A. (2003). Chk1-deficient tumour cells are viable but exhibit multiple checkpoint and survival defects. *EMBO J.* **22**, 713-723.

Zachos, G., Rainey, M. D. and Gillespie, D. A. (2005). Chk1-dependent S-M checkpoint delay in vertebrate cells is linked to maintenance of viable replication structures. *Mol. Cell. Biol.* **25**, 563-574.

Zhao, H. and Piwnica-Worms, H. (2001). ATR-mediated checkpoint pathways regulate phosphorylation and activation of human Chk1. *Mol. Cell. Biol.* **21**, 4129-4139.

Zou, L. and Elledge, S. J. (2003). Sensing DNA damage through ATRIP recognition of RPA-ssDNA complexes. *Science* **300**, 1542-1548.

Virus Genes
DOI 10.1007/s11262-009-0447-x

The PDZ domain binding motif (PBM) of human T-cell leukemia virus type 1 Tax can be substituted by heterologous PBMs from viral oncoproteins during T-cell transformation

Tomoya Aoyagi · Masahiko Takahashi · Masaya Higuchi · Masayasu Oie · Yuetsu Tanaka · Tohru Kiyono · Yutaka Aoyagi · Masahiro Fujii

Received: 28 July 2009 / Accepted: 30 December 2009

Abstract Several tumor viruses, such as human T-cell leukemia virus (HTLV), human papilloma virus (HPV), human adenovirus, have high-oncogenic and low-oncogenic subtypes, and such subtype-specific oncogenesis is associated with the PDZ-domain binding motif (PBM) in their transforming proteins. HTLV-1, the causative agent of adult T-cell leukemia, encodes Tax1 with PBM as a transforming protein. The Tax1 PBM was substituted with those from other oncoviruses, and the transforming activity was examined. Tax1 mutants with PBM from either HPV-16 E6 or adenovirus type 9 E4ORF1 are fully active in the transformation of a mouse T-cell line from interleukin-2-dependent growth into independent growth. Interestingly, one such Tax1 PBM mutant had an extra amino acid insertion derived from E6 between PBM and the rest of Tax1, thus suggesting that the amino acid sequences of the peptides between PBM and the rest of Tax1 and the numbers only slightly affect the function of PBM in the transformation. Tax1 and Tax1 PBM mutants interacted with tumor suppressors Dlg1 and Scribble with PDZ-domains. Unlike E6, Tax1 PBM mutants as well as Tax1 did not or minimally induced the degradations of Dlg1 and Scribble, but instead induced their subcellular translocation from the detergent-soluble fraction into the insoluble fraction, thus suggesting that the inactivation mechanism of these tumor suppressor proteins is distinct. The present results suggest that PBMs of high-risk oncoviruses have a common function(s) required for these three tumor viruses to transform cells, which is likely associated with the subtype-specific oncogenesis of these tumor viruses.

Keywords HTLV-1 · Tax · PDZ · PBM

Introduction

Human T-cell leukemia virus (HTLV) has two subtypes with distinct pathogenicities [1–3]. The type 1 virus (HTLV-1) is the etiologic agent of adult T-cell leukemia, whereas type 2 one (HTLV-2) is not associated with any malignancies. These two viruses immortalize human T-cells in vitro with equivalent efficiency. Therefore, the distinct pathogenicities are likely to be in the later step of the leukemogenesis [4]. Accumulating evidence suggests the crucial involvement of HTLV-1 Tax1 protein in the aggressive pathogenicity of HTLV-1 relative to HTLV-2 [5–8].

Tax1 and Tax2 are the transforming proteins of HTLV-1 and HTLV-2, respectively, which are essential for the viruses to immortalize human T-cells in vitro [7, 9–12]. Tax1 and Tax2 have multiple activities such as transcriptional activation of cellular genes through NF-κB, CREB/

Tomoya Aoyagi and Masahiko Takahashi contributed equally to this study.

T. Aoyagi · M. Takahashi · M. Higuchi · M. Oie · M. Fujii (✉)
Division of Virology, Graduate School of Medical and Dental Sciences, Niigata University, 1-757 Asahimachi-Dori, Niigata 951-8510, Japan
e-mail: fujiimas@med.niigata-u.ac.jp

T. Aoyagi · Y. Aoyagi
Division of Gastroenterology and Hepatology, Graduate School of Medical and Dental Sciences, Niigata University, 1-757 Asahimachi-Dori, Niigata 951-8510, Japan

Y. Tanaka
Department of Immunology, Graduate School and Faculty of Medicine, University of the Ryukyus, Okinawa, Japan

T. Kiyono
Virology Division, National Cancer Center Research Institute, Chuo-ku, Tokyo, Japan

Published online: 13 January 2010

ATF, SRF and AP-1 and the inactivation of tumor suppressor proteins p53 and p16INK4a [13–18], but they are generally equivalent to each other. Tax1 and Tax2 have, however, a significant difference in the transforming activities in vitro [5, 6]. For instance, Tax1 transforms a mouse T-cell line CTLL-2 from interleukin (IL)-2-dependent growth into independent growth, and the activity was much greater than that of Tax2 [6]. Subsequent studies identified two Tax1-specific activities responsible for the distinct transforming activities. One is the activity through the PDZ domain binding motif (PBM) present only in Tax1 but not in Tax2 [6, 19], and the other is the activation of transcription factor NF-κB2 [8]. Therefore, elucidating these differences would uncover the molecular mechanism underlying the distinct pathogenicities of these viruses.

Human papilloma virus (HPV) and human adenovirus are associated with human cervical cancer and estrogen-dependent mammary tumors in female rats, respectively. Interestingly, they also have high-oncogenic subtypes and low-oncogenic ones, and only the high-oncogenic subtypes have PBM in the transforming proteins such as E6 of HPV type 16 and E4ORF1 of adenovirus type 9 [20, 21]. Tax1 PBM mutants were produced either with HPV-16 E6 or E4ORF1 of adenovirus type 9 to examine whether these PBM are functionally substitutable in the functions. These heterologous PBMs from other high-pathogenic oncoviruses fully substituted for Tax1 PBM in the transformation. These results further supported the hypothesis that PBMs of viral oncoproteins have a common function in the transformation, and thus also in the subtype-specific oncogenesis of tumor viruses.

Materials and methods

Cells and culture conditions

293T cells are derived from the human embryonic kidney. This cell line was cultured in Dulbecco's modified Eagle's medium (DMEM) supplemented with 10% heat inactivated fetal bovine serum (FBS), 4 mM L-glutamine, penicillin (50 U/ml), and streptomycin (50 μg/ml) at 37°C in 5% CO_2. Human T-cell lines used in the present experiments have been characterized previously [19, 22]. Jurkat and MOLT-4 are HTLV-1-negative T-cell lines. MT-4 and SLB-1 are HTLV-1-infected human T-cell lines. These T-cell lines were cultured in RPMI1640 supplemented with 10% FBS, 4 mM L-glutamine, penicillin (50 U/ml), and streptomycin (50 μg/ml; RPMI/10%FBS). CTLL-2 is a mouse T lymphocyte cell line which was cultured in RPMI/10%FBS supplemented with 55 μM 2-mercaptoethanol and 500 pM recombinant human IL-2 (RPMI/10%FBS/IL-2) at 37°C in 5% CO_2.

Plasmids

The lentiviral vector CSII-EF-IG-RfA and the expression vector pHβPr-1-neo were used for the expression of Tax1 or its mutant proteins, as previously described [5, 8]. Tax1ΔC is a PBM-negative mutant and has four amino acid deletion from the C-terminus of Tax1 [19]. M1, M2, and M3 are Tax1 PBM mutants and have PBM from adenovirus type 9 E4ORF1 (ATLV), HPV-16 E6 (ETQL), and HPV-16 E6 (RSSRTRRETQL), respectively. The mutations were introduced using the polymerase chain reaction (PCR). The 3′-primers used for PCR were 5′-TC AGACAAGTGTAGCTCGGAAATGTTTTTCACT-3′ for M1, 5′-TCAAAGTTGTGTTTCTCGGAAATGTTTTTCA CT-3′ for M2, and 5′-TCAAAGTTGTGTTTCGCGGCGT GTGCGGCTGCTGCGTCGGAAATGTTTTTCACT For M3. The common 5′-primer was 5′-AACAGCTATGAC-CATG-3′ corresponding to the pBluescript-tax1 plasmid, which has the wild-type tax1 gene. After the mutations were confirmed by DNA sequencing, these genes were cloned into pENTR/D-TOPO (Invitrogen) and then were transferred to CSII-EF-IG-RfA by an LR recombination reaction using LR clonase (Invitrogen). In addition, the tax1 mutant genes were cloned into pHβPr-1-neo plasmid.

Cell lysate preparation

The 293T and human T-cell lines were treated with lysis buffer [1% NP40, 25 mM Tris–HCl (pH 7.2), 150 mM NaCl, 1 mM EDTA, 1 mM phenylmethylsulfonyl fluoride and 2 μg/ml leupeptin] at 4°C for 15 min to prepare detergent soluble and insoluble fractions. After centrifugation, the supernatant was collected and used as a soluble fraction, and the resultant pellet was suspended in sodium dodecyl sulfate (SDS) sample buffer [2% SDS, 62.5 mM Tris–HCl (pH 6.8), 20% glycerol, 0.01% bromophenol blue, 50 mM dithiothreitol], and then heated at 95°C for 5 min. After centrifugation, the supernatants were used as the insoluble fraction. To prepare total lysates, the cells were suspended with the SDS sample buffer and heated at 95°C for 5 min. After centrifugation, the supernatants were used as the total cell lysates.

Western blotting

Soluble fraction (30 μg), insoluble fraction (20 μg), and total cell lysates (20 μg) were size-separated on 6–12% polyacrylamide gel containing SDS and then were electronically transferred to the PVDF membranes. The membranes were incubated with the primary antibody, followed by the corresponding secondary antibody labeled with peroxidase, and then were visualized using an ECL Western blotting detection system (GE Healthcare). The

primary antibodies used were anti-Tax1 monoclonal antibody (TAXY-7) [23], anti-HA (HA-7 from Sigma), anti-Scribble (K-21, Santa Cruz Biotechnology, Santa Cruz, CA), mouse anti-Dlg1 monoclonal antibody (BD Biosciences Pharmingen, San Diego, CA), mouse anti-α-Tubulin monoclonal antibody (Calbiochem), and goat anti-Lamin B polyclonal antibody (Santa Cruz).

Co-immunoprecipitation assay

The co-immunoprecipitation assay was performed as described previously [24]. Briefly, the pHβPr-1-Tax1 or its mutant plasmids were transiently transfected into 293T cells by lipofection (Fugene6, Roche Molecular Systems, Peasanton, CA). Forty-eight hours after the transfection, the cells were treated with lysis buffer supplemented with 1 mM phenylmethylsulfonyl fluoride and 2 μg/ml leupeptin, and the lysates were cleared by centrifugation and immunoprecipitated with anti-Tax1 antibody (TAXY-7). The immunoprecipitated proteins were analyzed by Western blotting using anti-Scribble (K-21, Santa Cruz Biotechnology), anti-Dlg1 monoclonal antibody (BD Biosciences Pharmingen), and anti-Tax1, respectively. The antibody binding to the membrane was visualized using an ECL Western blotting detection system (GE Healthcare).

Transformation assay

Recombinant lentiviruses were generated by transfecting pCAG-HIVgp, pCMV-VSV-G-RSV-Rev (provided by H. Miyoshi) and the respective lentiviral vector plasmids (Tax1, Tax1ΔC, M1, M2, M3 in CSII-EF-IG-RfA) into 293T cells by using FuGENE6 (Roche). The supernatant containing the respective viruses was then infected into the CTLL-2 cells (5×10^5) in 2 ml of RPMI/10%FBS/IL-2 medium containing 8 μg/ml polybrene (Sigma). Forty-eight hours after infection, the cells were washed four times with phosphate-buffered saline (PBS), suspended in RPMI/10%FBS without IL-2, and cultured in a 96-well plate (3,000 cells/well, 5,000 cells/well, 10,000 cells/well) for 3 weeks. During the culture period, the medium was changed every three days. Next, the number of wells containing outgrowing cells was counted using a light microscope. The transformation (number) was then determined based on the number of positive wells out of 96 wells.

Immunostaining analysis

To analyze the subcellular localization of Tax1, Tax1 PBM mutants, Dlg1 and Scribble proteins in 293T cells, the cells were cultured on glass slides in 6-well culture plate overnight, and then the cells were transiently transfected with either the pHβPr-neo-Tax1, pHβPr-neo-Tax1ΔC, pHβPr-neo-Tax1M1, pHβPr-neo-Tax1M2 or pHβPr-neo-Tax1M3 plasmid using the lipofection method (FuGENE 6). At 48 h after transfection, the cells were fixed with 4% formaldehyde in PBS for 25 min at 4°C. The fixed cells were then incubated with the mouse anti-Dlg1 antibody (BD Biosciences Pharmingen) and the serum from an HTLV-1 carrier for Dlg1 analysis, or incubated with the rabbit anti-Scribble antibody (H-300) and the mouse anti-Tax1 antibody (TAXY-7) for a Scribble analysis. After washing, the cells were incubated with Alexa 594 labeled anti-mouse IgG (Molecular Probes, Eugene, OR) and fluorescein isothiocyanate labeled anti-human IgG (Beckman Coulter, Fullerton, CA) for Dlg1 analysis, or incubated with Alexa 594 labeled anti-mouse IgG (Molecular Probes) and Alexa 488 labeled anti-rabbit IgG (Molecular Probes) for a Scribble analysis. After washing, the cells were stained with Hoechst 33258. The stained cells were then examined by fluorescent microscopy (BZ-8000, KEYENCE).

Results

Functional substitution of Tax1 PBM by heterologous PBMs

Three Tax1 PBM mutants were produced to examine whether PBMs of other oncoproteins can substitute Tax1 PBM in the transformation. M1 and M2 have the PBM of adenovirus type 9 E4ORF1and HPV-16 E6 (ATLV and ETQL instead of ETEV in Fig. 1a), respectively. M3 has the 11 amino acid from the E6 C-terminus including PBM and thus have an extra seven amino acid residues relative to Tax1. The lentiviruses encoding these Tax1 mutants as well as Tax1ΔC without Tax1 PBM were cultured with an IL-2-dependent T-cell line (CTLL-2) for 24 h, and then cultured without IL-2 for 3 weeks on 96-well plates. The wells with outgrowing cells were counted by a light microscope. Cells infected with the control lentivirus or with lentivirus encoding Tax1ΔC without PBM did not induce the outgrowth of CTLL-2 cells (Fig. 1b). On the other hand, all three Tax1 PBM mutants efficiently induced the outgrowth, although the activities were not as strong as those of wild type Tax1. The inability of Tax1ΔC to transform CTLL-2 was not due to the quantity of the Tax1ΔC proteins in CTLL-2, since a Western blotting analysis detected the equivalent amount of Tax1ΔC protein to those of Tax1 in CTLL-2 (Fig. 1c). It should be noted that a substitution mutation of Tax1 amino acid 353 from Val to Ala (Tax353A) or 351 from Thr to Ala (Tax351A) abrogated the transforming activity [6], denying that the addition of any four amino acids to Tax1 C-terminus can rescue the transforming activity. Therefore, these results

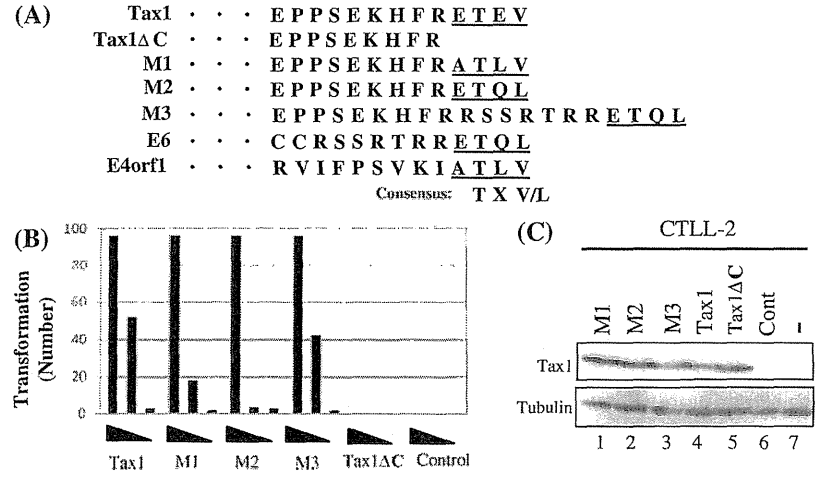

Fig. 1 The functional substitution of Tax1 PBM by heterologous PBMs of viral oncoproteins. **a** Amino acid sequences of the C-terminal ends of three oncoproteins and Tax1 mutants. **b** The cell lysates were prepared from CTLL-2 cells infected with lentiviruses encoding the indicated Tax1 mutants or the control lentivirus (Cont), and they were characterized by a Western blotting analysis using anti-Tax1 antibody. **c** CTLL-2 cells were infected with lentiviruses encoding Tax1 or the indicated Tax1 mutants, or the control lentivirus (Cont). They were cultured with IL-2 for 24 h, washing with PBS, and then cultured without IL-2 for 3 weeks on 96-well plate in the density of 1,000 cells/well, 3,000 cells/well or 10,000 cells/well. The wells containing outgrowing cells were counted by a light microscope. The transformation (number) is the number of wells containing outgrowing cells (the maximum number is 96)

indicated that the PBM from two oncoviruses can substitute for the function of the Tax1 PBM in the transformation. Unlike other PBM mutants, M3 has extra amino acid residues in front of PBM derived from E6 (Fig. 1a), thus indicating that PBM can flexibly perform its function(s) in the transformation.

Tax1 mutants interact with PDZ domain proteins

Tax1 is known to interact with multiple PDZ domain proteins including Dlg1 and Scribble [24–26], and the interactions are strongly correlated with the transforming activity toward CTLL-2 [22]. Tax1 expression plasmids were transfected into 293T cells. The lysates prepared from the transfected cells were then immunoprecipitated with anti-Tax1 antibody, and the proteins precipitated with Tax1 were characterized with anti-Dlg1 or anti-Scribble antibody. Anti-Tax1 antibody co-immunoprecipitated endogenous Dlg1 and Scribble together with wild type Tax1 or its PBM mutants (M1, M2, M3), but not with Tax1ΔC, thus indicating that Dlg1 and Scribble interact with Tax1 mutants in a heterologous PBM-dependent manner (Fig. 2). In addition, the amount of Dlg1 and Scribble in soluble cell lysates was reduced by the interaction with Tax1 and its mutant. A previous study showed that Dlg1 is translocated to the detergent insoluble fraction through binding to Tax1 [19]. Three cell lysates (namely, the detergent soluble fraction, the detergent insoluble fraction, the total lysate) were prepared from the 293T cells transfected with the Tax1 plasmids used above to examine whether Tax1 has similar activity to Scribble. While Tax1 or its mutants interacting with these PDZ domain proteins

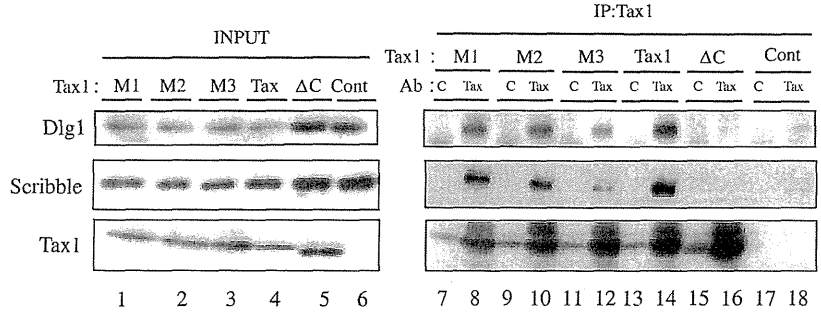

Fig. 2 Tax1 PBM mutants can interact with Dlg1 and Scribble. Cell lysates were prepared from 293T cells transfected with the expression plasmids encoding the indicated Tax1 mutants or the control plasmid (*Cont*). An aliquot of the lysates were immunoprecipitated with anti-Tax1 antibody (*Tax*) or the control antibody (*C*). The total cell lysates (*Input*) and immunoprecipitates (*IP*) were characterized by a Western blot analysis using anti-Dlg1, anti-Scribble, or anti-Tax1 antibody

reduced the amounts of Dlg1 and Scribble in the soluble fraction, they increased those in the insoluble fraction (Fig. 3). Since Tax1 or its mutants had little effect on the amount of Dlg1 and Scribble in the total lysates, these results indicated that Tax1 changes the subcellular localization of Scribble as well as Dlg1 from the detergent soluble fraction into the insoluble one. In addition, Tax1 induced a slower-migrating form of Dlg1 in the insoluble and total fraction (lanes 7–10 in Fig. 3). This is likely to be due to the phosphorylation of Dlg1 described previously [25].

To further establish the interaction of Dlg1 and Scribble with the Tax1 mutants, their subcellular localizations in the absence or presence of Tax1 were examined by immunostaining. In 293T cells, endogenous Dlg1 and Scribble was localized primarily at the plasma membrane (Fig. 4). The transiently transduced Tax1 was localized in the nucleus and in the cytoplasm, and some were colocalized with Dlg1 and Scribble at the perinuclear region as large granules that were not observed without Tax1. Tax1ΔC was localized in the nucleus and in the cytoplasm and formed large granules at the perinuclear regions similar to that observed in Tax1, but these granules contained neither Dlg1 nor Scribble. These results suggested that Tax1 was colocalized with endogenous Dlg1 and Scribble in a PBM-dependent manner. Similar to Tax1, M2 was also colocalized with Dlg1 and Scribble at the perinuclear regions as large granules. On the other hand, the colocalization of M1 only with Dlg1, but not Scribble, was detected, and the colocalization of M3 neither with Dlg1 nor Scribble were detected. Since M1 and M3 as well as Tax1 interacted with both endogenous Dlg1 and Scribble in an immunoprecipitation assay (Fig. 2), these results may therefore indicate that M1 and M3 transiently interact with Dlg1 and Scribble; however, the amounts of which remains at undetectable levels based on an immunostaining assay.

To examine the effect of Tax1 on the localization of Dlg1 and Scribble in HTLV-1-infected T-cell lines, cell lysates were prepared from the indicated T-cell lines. Consistently with the transient transfection of Tax1 into 293T cells, HTLV-1-infected T-cell lines (MT-4, SLB-1) showed a reduced amount of Dlg1 and Scribble in the soluble fraction and an increased amount in the insoluble fraction in comparison to HTLV-1-uninfected T-cell lines (Jurkat, MOLT-4; Fig. 5). These results suggested that Tax1 in HTLV-1-infected T-cell lines is likely to induce the translocation of Dlg1 and Scribble from the detergent soluble fraction into the insoluble one.

Discussion

Subgroups of HTLV, HPV, and human adenovirus have oncoproteins with PBM, and the motif is associated with their oncogenic potentials in vivo. However, whether one motif has substitutable function(s) with the other PBMs has not been clarified. The present study showed that two different PBMs from HPV-16 E6 and E4ORF1 of human adenovirus type 9 can substitute the function of Tax1 PBM

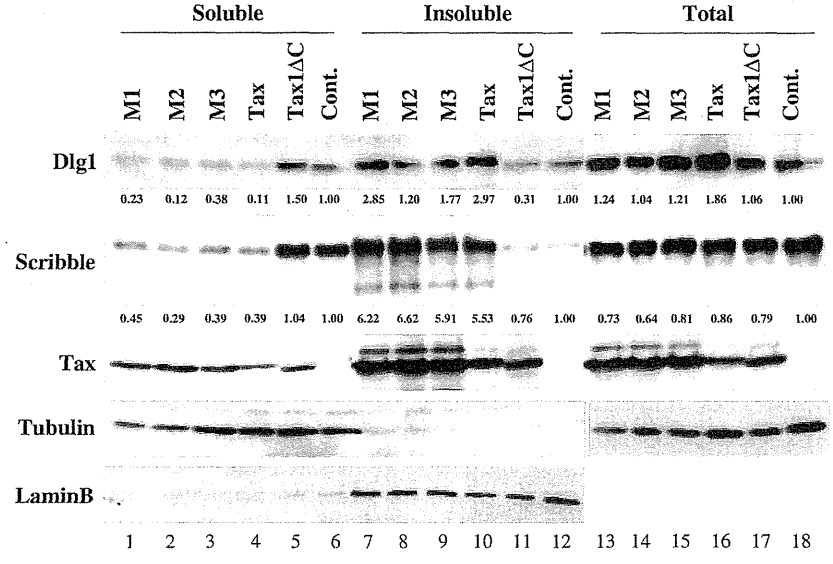

Fig. 3 Tax1 PBM mutants induce the subcellular translocation of Dlg1 and Scribble. Soluble, insoluble and total cell lysates were prepared from 293T cells transfected with the expression plasmids encoding the indicated Tax1 mutant or the control plasmid (*Cont*) as described in the Materials and methods. The lysates were characterized by a Western blotting analysis using anti-Dlg1, anti-Scribble, or anti-Tax1 antibody. The intensities of the respective bands were measured by a densitometer (Gel-Doc; Bio-Rad), and the numbers beneath the bands were calculated as a ratio of the intensity of the band in question relative to that of the Control (*Cont*)

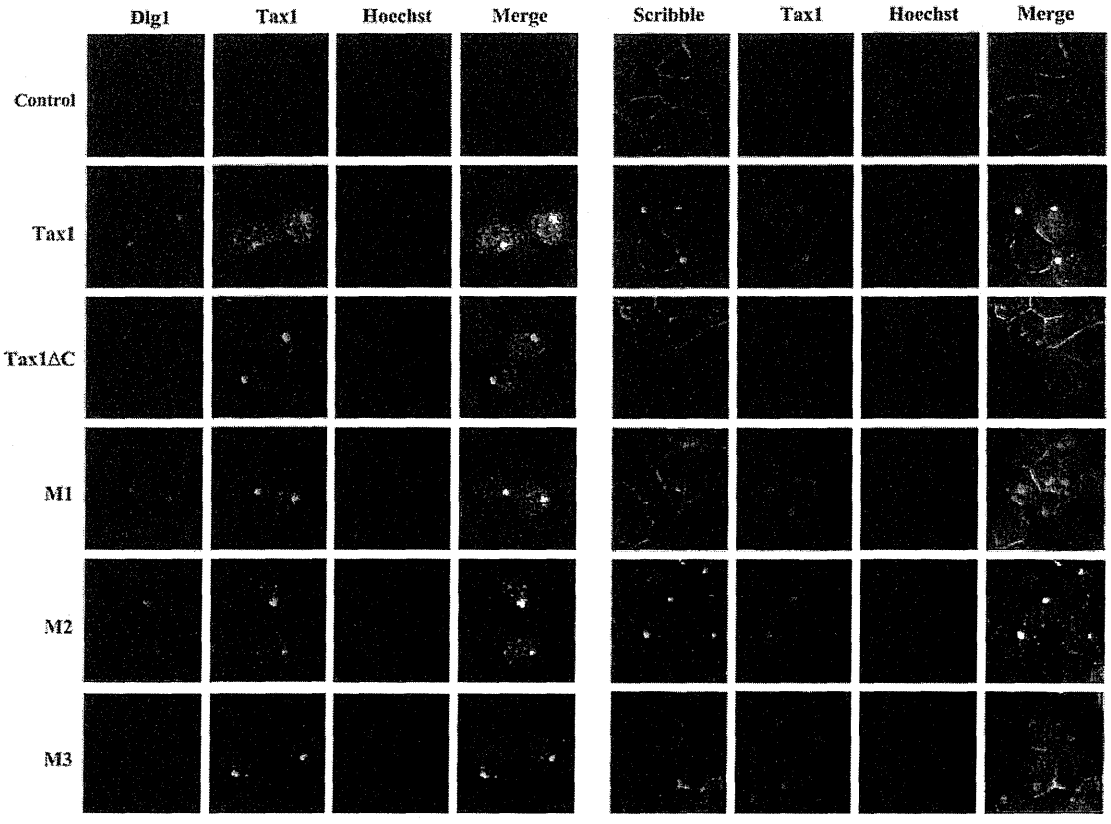

Fig. 4 Colocalization of Tax1 with Dlg1 and Scribble. 293T cells were transfected with either the pHβPr-neo-Tax1, pHβPr-neo-Tax1ΔC, pHβPr-neo-Tax1M1, pHβPr-neo-Tax1M2 or pHβPr-neo-Tax1M3 plasmid using the lipofection method. At 48 h after transfection, the cells were fixed and were stained with anti-Tax1 and with Hoechst 33258 together either with anti-Dlg1 or anti-Scribble. The stained cells were examined using fluorescent light microscopy

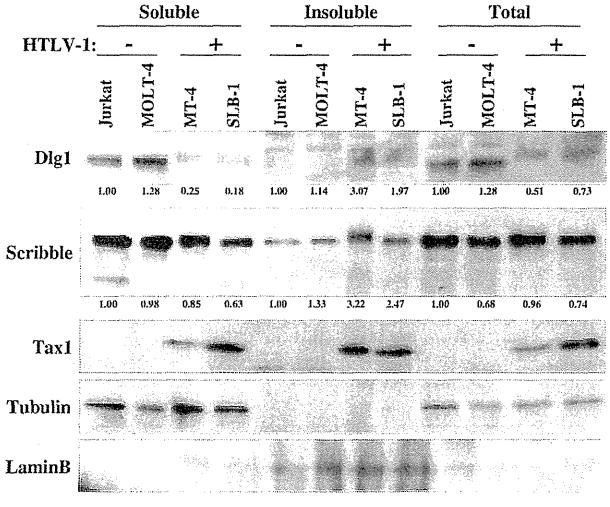

Fig. 5 Expression of Dlg1 and Scribble in human T-cell lines. Soluble, insoluble and total cell lysates were prepared from the indicated human T-cell lines as described in Materials and methods. The lysates were characterized by a Western blot analysis using anti-Dlg1, anti-Scribble, or anti-Tax1 antibody. HTLV-1 infection to the cell lines was indicated. The intensities of the respective bands were measured by a densitometer (Gel-Doc; Bio-Rad), and the numbers beneath the bands were calculated as a ratio of the intensity of the band in question relative to that of Jurkat

in the transformation toward a T-cell line. Therefore, these results suggest that the motif has common function(s) in the transforming activities, thus indicating that they may play a role in the subtype-specific oncogenesis.

Three Tax1 PBM mutants, through direct interaction, induced the subcellular translocation of Dlg1 and Scribble from a soluble fraction into an insoluble one, and the amounts of such translocation were more than half of the proteins and the activities were equivalent to those of wild type Tax1 (Figs. 2 and 3). On the other hand, an immunostaining assay showed that M3 interacted neither with Dlg1 nor Scribble, and M1 only interacted with Dlg1 (Fig. 4). Therefore, the activities of Tax1 and its mutants to induce the translocations of Dlg1 and Scribble did not correlate with their colocalizations with Dlg1 and Scribble. These results suggest that M1 and M3 (and possibly Tax1 and M2 also) transiently interact with Dlg1 and Scribble, which induce their translocations, although a further analysis is required to establish this hypothesis.

M3, a Tax1 PBM mutant, has an extra seven amino acid residues relative to wild type Tax1, derived from E6 (Fig. 1a); nevertheless, the transforming activity of M3 was equivalent to that of Tax1. This result was unexpected,

since the Tax1 C-terminal amino acid residues close to the PBM are well conserved among HTLV-1 isolates but it is dissimilar to E6. Therefore, these results indicated that the PBM is structurally and functionally independent from the other part of Tax1.

While E6 induces the degradation of Dlg1 and Scribble in a PDZ-dependent manner [21], Tax1 did not or minimally induce the degradation of Dlg1 and Scribble in 293T cells, and instead it altered the subcellular localization of Dlg1 and Scribble from the soluble fraction into the insoluble fraction (Fig. 3). This is consistent with the previous study that Tax1 induces the translocation of Dlg1 from the soluble fraction into the insoluble fraction [19]. Therefore, both Tax1 and E6 are thought to inactivate these tumor-suppressor PDZ domain proteins [25], but the mechanisms may be distinct from each other. Interestingly, two Tax1 mutants with E6 PBM also did not (or minimally) induce the degradation of Dlg1 and Scribble. As a result, the region(s) of E6, other than PBM, is thus considered to be a main determinant for inducing the degradation of Dlg1 and Scribble probably by means of binding to a ubiquitin ligase, namely, E6-AP [27]. Attempts to compare the activities of Tax1 and E6 to Dlg1 and Scribble in cells were unsuccessful, since expression of E6 from the expression plasmid in 293T cells was much lower than that of Tax1 (data not shown). Thus, a further analysis is required to establish the mechanisms of Tax1 and E6 to inactivate these PDZ domain proteins.

Acknowledgments We would like to thank Dr. Hiroyuki Miyoshi at RIKEN Tsukuba Institute for providing the lentivirus plasmids. We also wish to thank the Takeda Pharmaceutical Company for providing recombinant human IL-2. We would like to express our gratitude to Misako Tobimatsu for her excellent technical assistance. This work was supported in part by a Grant-in-Aid for Scientific Research on Priority Areas and for Scientific Research (C) of Japan, as well as a Grant for the Promotion of Niigata University Research Projects.

References

1. Y. Hinuma, K. Nagata, M. Hanaoka, M. Nakai, T. Matsumoto, K.I. Kinoshita, S. Shirakawa, I. Miyoshi, Proc. Natl. Acad. Sci. USA **78**(10), 6476–6480 (1981)
2. T. Uchiyama, Annu. Rev. Immunol. **15**, 15–37 (1997)
3. R.C. Gallo, Retrovirology **2**(1), 17 (2005)
4. G. Feuer, P.L. Green, Oncogene **24**(39), 5996–6004 (2005)
5. K. Endo, A. Hirata, K. Iwai, M. Sakurai, M. Fukushi, M. Oie, M. Higuchi, W.W. Hall, F. Gejyo, M. Fujii, J. Virol. **76**(6), 2648–2653 (2002)
6. C. Tsubata, M. Higuchi, M. Takahashi, M. Oie, Y. Tanaka, F. Gejyo, M. Fujii, Retrovirology **2**, 46 (2005)
7. W.W. Hall, M. Fujii, Oncogene **24**(39), 5965–5975 (2005)
8. M. Higuchi, C. Tsubata, R. Kondo, S. Yoshida, M. Takahashi, M. Oie, Y. Tanaka, R. Mahieux, M. Matsuoka, M. Fujii, J. Virol. **81**(21), 11900–11907 (2007)
9. R. Grassmann, S. Berchtold, I. Radant, M. Alt, B. Fleckenstein, J.G. Sodroski, W.A. Haseltine, U. Ramstedt, J. Virol. **66**(7), 4570–4575 (1992)
10. T. Akagi, K. Shimotohno, J. Virol. **67**(3), 1211–1217 (1993)
11. T.M. Ross, S.M. Pettiford, P.L. Green, J. Virol. **70**(8), 5194–5202 (1996)
12. C.Z. Giam, K.T. Jeang, Front. Biosci. **12**, 1496–1507 (2007)
13. S.L. Cross, M.B. Feinberg, J.B. Wolf, N.J. Holbrook, F. Wong-Staal, W.J. Leonard, Cell **49**(1), 47–56 (1987)
14. M. Maruyama, H. Shibuya, H. Harada, M. Hatakeyama, M. Seiki, T. Fujita, J. Inoue, M. Yoshida, T. Taniguchi, Cell **48**(2), 343–350 (1987)
15. M. Fujii, H. Tsuchiya, T. Chuhjo, T. Akizawa, M. Seiki, Genes Dev. **6**(11), 2066–2076 (1992)
16. L.J. Zhao, C.Z. Giam, Proc. Natl. Acad. Sci. USA **89**(15), 7070–7074 (1992)
17. T. Suzuki, T. Narita, M. Uchida-Toita, M. Yoshida, Virology **259**(2), 384–391 (1999)
18. K. Iwai, N. Mori, M. Oie, N. Yamamoto, M. Fujii, Virology **279**(1), 38–46 (2001)
19. A. Hirata, M. Higuchi, A. Niinuma, M. Ohashi, M. Fukushi, M. Oie, T. Akiyama, Y. Tanaka, F. Gejyo, M. Fujii, Virology **318**(1), 327–336 (2004)
20. S.S. Lee, R.S. Weiss, R.T. Javier, Proc. Natl. Acad. Sci. USA **94**(13), 6670–6675 (1997)
21. R.T. Javier, Oncogene **27**(55), 7031–7046 (2008)
22. K. Ishioka, M. Higuchi, M. Takahashi, S. Yoshida, M. Oie, Y. Tanaka, S. Takahashi, L. Xie, P.L. Green, M. Fujii, Retrovirology **3**, 71 (2006)
23. Y. Tanaka, A. Yoshida, H. Tozawa, H. Shida, H. Nyunoya, K. Shimotohno, Int. J. Cancer **48**(4), 623–630 (1991)
24. M. Okajima, M. Takahashi, M. Higuchi, T. Ohsawa, S. Yoshida, Y. Yoshida, M. Oie, Y. Tanaka, F. Gejyo, M. Fujii, Virus Genes **37**(2), 231–240 (2008)
25. T. Suzuki, Y. Ohsugi, M. Uchida-Toita, T. Akiyama, M. Yoshida, Oncogene **18**(44), 5967–5972 (1999)
26. C. Arpin-Andre, J.M. Mesnard, J. Biol. Chem. **282**(45), 33132–33141 (2007)
27. Y. Matsumoto, S. Nakagawa, T. Yano, S. Takizawa, K. Nagasaka, K. Nakagawa, T. Minaguchi, O. Wada, H. Ooishi, K. Matsumoto, T. Yasugi, T. Kanda, J.M. Huibregtse, Y. Taketani, J. Med. Virol. **78**(4), 501–507 (2006)

Biomedical Research 31 (3) 199-206, 2010

Expression of a chemokine BRAK/CXCL14 in oral floor carcinoma cells reduces the settlement rate of the cells and suppresses their proliferation *in vivo*

Shin Ito[1, 2], Shigeyuki Ozawa[1, 2, 3], Takeharu Ikoma[1, 2], Nobuyuki Yajima[1, 2], Tohru Kiyono[4], and Ryu-Ichiro Hata[1, 2]

[1] Oral Health Science Research Center, [2] Department of Biochemistry and Molecular Biology, [3] Department of Oral and Maxillofacial Surgery, Kanagawa Dental College, 82 Inaoka-cho, Yokosuka, 238-8580, and [4] Virology Division, National Cancer Center Research Institute, Tokyo, 104-0045, Japan

(Received 23 March 2010; and accepted 12 May 2010)

ABSTRACT

We reported previously that the forced expression of the chemokine BRAK/CXCL14 in head and neck squamous cell carcinoma cells decreased the rate of tumor formation and size of tumor xenografts in athymic nude mice and SCID mice. In order to clarify the expression of BRAK/CXCL14 affected either the settlement of carcinoma cells in host tissues *in vivo* or proliferation of the colonized carcinoma cells or both, we prepared oral floor carcinoma-derived HSC-2 cells in which BRAK/CXCL14 expression was induced upon doxycycline treatment. Then 30 nude mice were separated into 3 groups composed of 10 mice per group: Group I, the control, in which the engineered cells were directly xenografted onto the back of the mice; Group II, the cells were xenografted and then the mice were treated with doxycycline; and Group III, the cells were pretreated with doxycycline during culture, and the host mice were also treated with the drug before and after xenografting. The effects of BRAK/CXCL14 expression were examined by measuring the tumor size. The order of the size of tumor xenografts was Group I > II > III, even though the growth rate of the engineered cells was the same whether or not the cells were cultured in the presence of the drug. In addition, the size of tumors was significantly down-regulated after xenografting the doxycycline-pretreated cells in Group III. These data indicate that BRAK/CXCL14 expression in oral floor carcinoma cells reduced both the rate of settlement and the proliferation of the cells *in vivo* after settlement of the cells.

Chemokines are a family of small (8–14 kDa) mostly basic, structurally related chemotactic cytokines, and they function as leukocyte subtype-selective chemo-attractants (29, 30). A complex network of chemokines and their receptors influences the development of primary tumors and metastasis (2, 19, 29).

First detected in breast and kidney, BRAK is also called CXC chemokine ligand 14 (CXCL14), and was reported to induce B cell, monocyte (26), and dendritic cell infiltration into normal and tumour tissues (25) and to inhibit angiogenesis (23). Generally, BRAK/CXCL14 is expressed universally and abundantly in normal tissues but is absent from or expressed only in a very small amount in cancerous tissues *in vivo* and in carcinoma cells in culture, including head and neck squamous cell carcinoma (HNSCC) cells (7, 9, 11, 16, 23). On the other hand, heightened BRAK/CXCL14 expression has been reported to occur in adenocarcinomas such as prostate (22), breast cancer (1) and pancreatic cancer cells (28). These data suggest that the effects of BRAK/CXCL14 on the development and progression of cancer might be quite different between HN-

Address correspondence to: Dr. Ryu-Ichiro Hata, Oral Health Science Research Center, Kanagawa Dental College, 82 Inaoka-cho, Yokosuka, 238-8580, Japan
Tel: +81-46-822-9587, Fax: +81-46-822-9587
E-mail: ryuhata@gmail.com

SCC and adenocarcinoma.

We reported previously that the forced expression of BRAK/CXCL14 in tongue carcinoma cells decreased the rate of tumor formation and size of tumor xenografts in athymic nude mice (16) and SCID mice (17). In these experiments on cloned cells with an upregulated BRAK/CXCL14 protein expression, the growth of these cells under culture conditions was the same as that of control mock vector-transfected cells. However, the migration rate of the BRAK/CXCL14-expressing cells *in vitro* was significantly slower than that of the mock-vector transfected cells and attachment of the cells to collagen was much faster than the control cells (21).

Recent progress in cancer research has shown that cancerous tissues *in vivo* are derived from colonies of cancer stem cells (3, 10, 14, 18). These data raised 3 possibilities regarding the apparent slower growth rate of xenografted BRAK/CXCL14-expressing tumor cells. The first is that the ratio of stem cell-like cells among the BRAK/CXCL14-expressing cells was smaller, and thus a smaller number of carcinoma cells settled in the tissues of the host mice. The second possibility is that the growth rate of BRAK/CXCL14-expressing cells *in vivo* was slower than that of mock-vector transfected cells. The third one is that both the rate of settlement and proliferation of the cells *in vivo* after settlement of the cells was reduced.

In order to assess either BRAK/CXCL14 expression in tumor cells regulates settlement of tumor cells in the tissue or proliferation of the colonized tumour cells or both, we employed doxycycline-inducible HSC-2 cells, which express a high amount of BRAK/CXCL14 proteins only in the presence of doxycycline (8), a derivative of tetracycline (24), referred to Tet-on BRAK HSC-2 cells.

MATERIALS AND METHODS

Materials. Dulbecco's modified Eagle's medium was obtained from Sigma (Tokyo, Japan), and gentamicin sulfate, Trypsin 250 and sucrose were from Wako Pure Chemical Industries (Osaka, Japan). Mg^{2+}-Ca^{2+}-free phosphate-buffered saline tablets PBS (−) and doxycycline were purchased from TAKARA BIO (Shiga, Japan). Fungizone came from Invitrogen (Carlsbad, CA, USA); and fetal bovine serum (FBS) from Thermo Electron (Melbourne, Australia). TetraColor ONE reagent for determination of cell proliferation was from Seikagaku Corporation (Tokyo, Japan).

Construction of Tet-on BRAK vector and preparation of Tet-on BRAK HSC-2 cells. CSII-TRE-Tight-RfA was generated by replacing the EF1a promoter in CSII-EF-RfA (a gift from Dr. H. Miyoshi, RIKEN) with a tetracycline-inducible promoter, TRE-Tight, from pTRE-Tight (Clontech). Lentiviral vector plasmid, CSII-TRE-Tight-EGFP was constructed by recombination using the Gateway system (Invitrogen) as described previously (18). The HS4 chromatin insulator from the chicken β-globin locus control region (4) was inserted into the BspE1 site in the 3'-LTR of CSII-TRE-Tight-EGFP to generate CSII(ins)-TRE-Tight-EGFP. CSII(ins)-TRE-Tight-DEST was constructed by recombination between CSII(ins)-TRE-Tight-EGFP and pDONR221. BRAK cDNA was amplified by PCR and first recombined into pDONR221 and then recombined into CSII(ins)-TRE-Tight-DEST to generate CSII(ins)-TRE-Tight-BRAK.

The recombinant lentiviruses with the vesicular stomatitis virus G glycoprotein were produced as described previously (12). Production of recombinant retroviruses was described elsewhere (13). HSC-2 cells were infected with PQCXIN-TetON retroviruses and selected in the presence of G418 (800 μg/mL). The Tet-on HSC-2 cells were then infected with CSII(ins)-TRE-Tight-BRAK or enhanced green fluorescent protein (EGFP) expressing lentiviruses at the multiplicity of infection of more than 5 so as to generate Tet-on BRAK- and Tet-on EGFP-HSC-2 cells, respectively.

Cells and cell culture. HSC-2 cells derived from an oral floor carcinoma were obtained from the Japanese Collection of Research Bioresources (JCRB). The cells were cultured in Dulbecco's modified Eagle's medium containing gentamicin sulfate (50 mg/L), Fungizone (250 mg/L) and 10% FBS in the absence or the presence of various concentrations of doxycycline. The cells were cultured at 37°C under 95% air and 5% CO_2 and routinely passaged by treatment with 0.25% trypsin/1 mM ethylenediaminetetraacetic acid in PBS (−). The growth rate of the cells was determined by TetraColor ONE assay or by measuring the number of cells with a Coulter ZI Counter (Coulter Electronics Ltd., England).

Western blot analysis. We determined BRAK/CXCL14 and β-actin protein levels by using Western blotting as previously reported (16). Cells were lysed with Laemmli buffer consisting of 62.5 mM Tris-HCl (pH 6.8) containing 2% SDS, 8% glycerol,

0.05% bromophenol blue and 5% 2-mercaptoethanol. The proteins were separated by electrophoresis in an SDS-15–20% polyacrylamide gel (SuperSep; Wako Pure Chemical Industries, Osaka, Japan) and transferred onto an Immobilon-P membrane at a constant voltage of 50 volts for 2 h. After blocked with Odyssey Blocking Buffer (LI-COR Biosciences, Lincoln, NE), the membrane was incubated for 1 h at room temperature with appropriate primary antibodies in TBS solution [20 mM Tris-HCl (pH 7.6) containing 137 mM NaCl and 0.05% Tween-20]. It was then incubated with horseradish peroxidase (HRP)-conjugated sheep anti-mouse IgG, as the secondary antibody, for 30 min at room temperature. Immunoreactive bands were visualized using Lumi-Light Western Blotting Substrate (Roche Diagnostics, Tokyo, Japan). Intensity of signals on the Western blot was calculated by Image Quant 5.1 (GE Healthcare, Tokyo, Japan).

Tumor growth in vivo. Cells (1×10^7 cells/site) were injected subcutaneously into female BALB/c nu/nu mice (specific pathogen-free; Clea Japan, Tokyo, Japan). The mice were kept under a 12-h light/ 12-h dark cycle and provided water containing 2-mg/mL doxycycline and 5% (w/v) sucrose or 5% sucrose solution only for control mice (24). Tumor volume was calculated according to the following formula: $(a \times b^2)/2$, where "a" is the longer and "b" is the shorter dimension (16). All animal experiments in this study complied with the Guidelines of the Care and Use of Laboratory Animals of Kanagawa Dental College.

Immunohistochemical procedures. Tumor xenografts were removed from the mice and embedded in O.C.T compound (Tissue-Tek; Miles Inc., Elkhart, IN) and kept at −80°C. The frozen tissues were sectioned with a cryostat at 6 μm and the air-dried sections were incubated with rat anti-CD31antibody (ER-MP12; BMA Biomedicals, Switzerland, 1 : 800 dilution) as the 1st antibody and then with biotinylated rabbit anti-rat IgG (Vector Laboratories, Inc., Burlingame, CA; 1 : 250 dilution) as the 2nd antibody. Other sections were incubated with rabbit anti-α smooth muscle actin antibody (E184; Epitomics, Inc., Burlingame, CA; 1 : 100 dilution) as the 1st antibody followed by HRP-linked donkey anti-rabbit IgG (GE Healthcare, England; 1 : 50 dilution) as the 2nd antibody. For some sections the 1st antibody was omitted and used for a negative control. Histochemical color development was achieved by Vectastatin DAB (3,3'-diaminobenzidine) substrate kit (Vector Laboratories, Inc. Burlingame, CA) according to the manufacturer's instructions, as described previously (27). Areas positively stained with anti-CD31 or anti-α smooth muscle actin antibodies were measured in 5 randomly chosen visual fields at ×200 magnification by use of a Biozero microscope (KEYENCE, Tokyo, Japan) and VH analyzer software (KEYENCE).

Statistical analysis. Student's *t*-test was used to assess statistically significant differences between 2 groups *in vitro* cell growth and *in vivo* tumor volumes with $P < 0.05$ being considered statistically significant. The Smirnov-Grubbs test was also used to determine statistically significant differences in the size of xenografted tumors.

RESULTS

Production and characterization of Tet-on BRAK HSC-2 cells

We first tried to produce doxycycline-inducible BRAK-expressing cells by using a commercially available two-step system that employs transfection reagents; however, we could not obtain cells expressing BRAK/CXCL14 protein at a high enough level to be detected by Western blotting. Thus we prepared doxycycline-inducible BRAK-expressing cells using retrovirus- and lentivirus-mediated gene transfer. Tet-on BRAK HSC-2 cells obtained here expressed BRAK/CXCL14 in both time- and doxycycline dose-dependent manners; and over a 10 times higher level of BRAK protein was expressed after 24 h of treatment with 0.1 μg/mL of doxycycline than obtained without the drug (Fig. 1A and B). In addition 100% of the cells expressed EGFP as observed under a fluorescence microscope when Tet-on EGFP HSC-2 cells were cultured in the presence of doxycycline (data not shown).

The addition of various amounts of doxycycline to the culture medium of parental HSC-2 cells did not affect the growth rate of the cells (Fig. 2A). Furthermore, the growth rate of Tet-on BRAK HSC-2 cells was not affected by the presence of 0.1 μg/mL doxycycline up-to 8 days (Doxy; Fig. 2B), at which time the cells expressed 14 times more BRAK/CXCL14 than the control (see Fig. 1B), indicating that the presence of exogenously added doxycycline or the expression of over a 10 times higher level of BRAK/CXCL14 proteins by the cells did not affect the growth of the tumor cells under the culture conditions used.

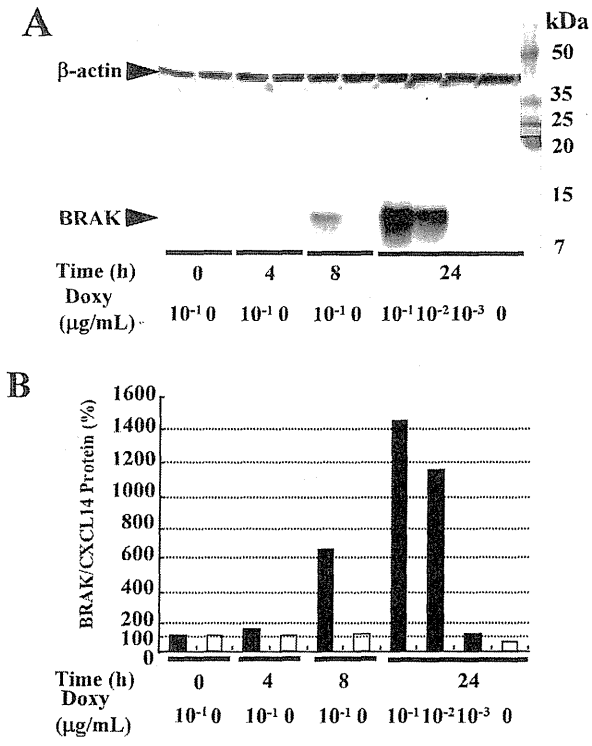

Fig. 1 Time- and doxycycline dose-dependent expression of BRAK/CXCL14 protein in Tet-on BRAK HSC-2 cells *in vitro*. The cells were cultured in the presence or absence of various concentrations of doxycycline (Doxy). (A) Proteins in the whole-cell lysates were separated by electrophoresis in SDS/15–20% polyacrylamide gels. BRAK/CXCL14 and β-actin proteins were visualized by performing Western blotting using respective antibodies. (B) The amounts of protein were determined by densitometry of the membrane shown in "A". Open columns indicate the cells cultured in the absence of doxycycline; and closed columns, those cultured in the presence of the drug.

Effects of expression of BRAK protein by Tet-on BRAK HSC-2 cells in vivo

In order to examine the effect of BRAK expression on the growth of HSC-2 cells *in vivo*, we injected Tet-on BRAK HSC-2 cells subcutaneously into mice. After 13 days, when the average size of tumors had reached 200 mm^3, we changed the drinking water from 5% sucrose solution [Group I: Doxy (−, −)] to 2 mg/mL doxycycline-containing 5% sucrose solution [Group II: Doxy (−, +)]. The growth of tumors was significantly slower in the doxycycline-treated mice than in the control animals (Fig. 3A), and tumors obtained from the former expressed a significantly higher amount of BRAK protein, as observed by Western blotting (Fig. 3B). When Tet-on BRAK HSC-2 cells were precultured for 7 days in the presence of 0.1 μg/mL of doxycycline before being injected into doxycycline-treated animals, the sizes of tumors at 6 days were significantly smaller than those at 3 days after the injection [Fig. 3A, Group III Doxy (+, +), see bracketed value], indicating that BRAK/CXCL14 expression affected the settlement of tumor cells. The sizes of tumors of Group III were always smaller than those of the tumors of doxycycline non-treated animals (Fig. 3A, Group I) and also those of animals treated with the drug after tumor cell injection (Fig. 3A, Group II). Also, the expression level of BRAK/CXCL14 protein in the tumors from the doxycycline-treated animals was significantly higher than that of controls at 34 days after transplantation (Fig. 3B). These finding thus indicate that BRAK/CXCL14 expression affected both the settlement of tumor cells and proliferation of the colonized cells.

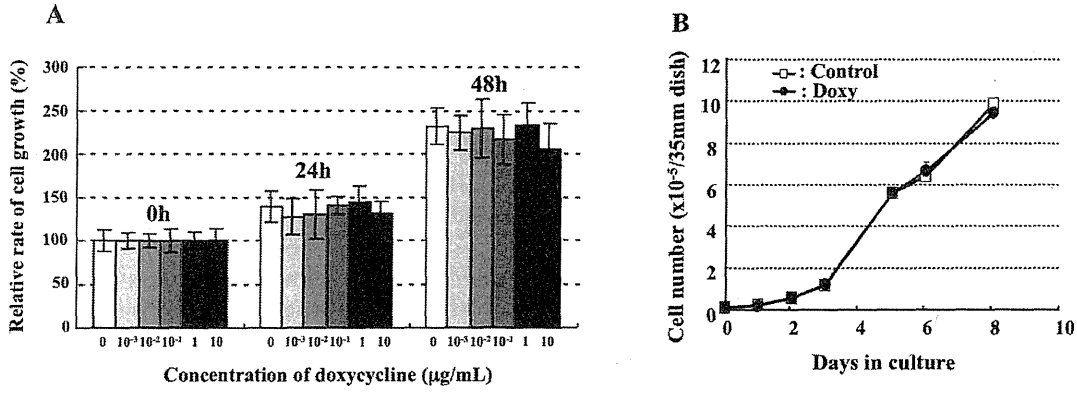

Fig. 2 Effect of doxycycline on the growth of cells. (A) HSC-2 cells (5×10^3/well) were plated on well bottom of a 96-well plate and cultured in the absence or presence of various concentrations of doxycycline for 0 to 48 h. The numbers of cells was determined by use of TetraColor One reagent. (B) Tet-on BRAK HSC-2 cells (2×10^4/35 mm dish) were plated and cultured for 8 days in the absence (open squares) or presence (closed circles) of doxycycline (0.1 μg/mL) and the number of cells was determined with a Coulter Counter.

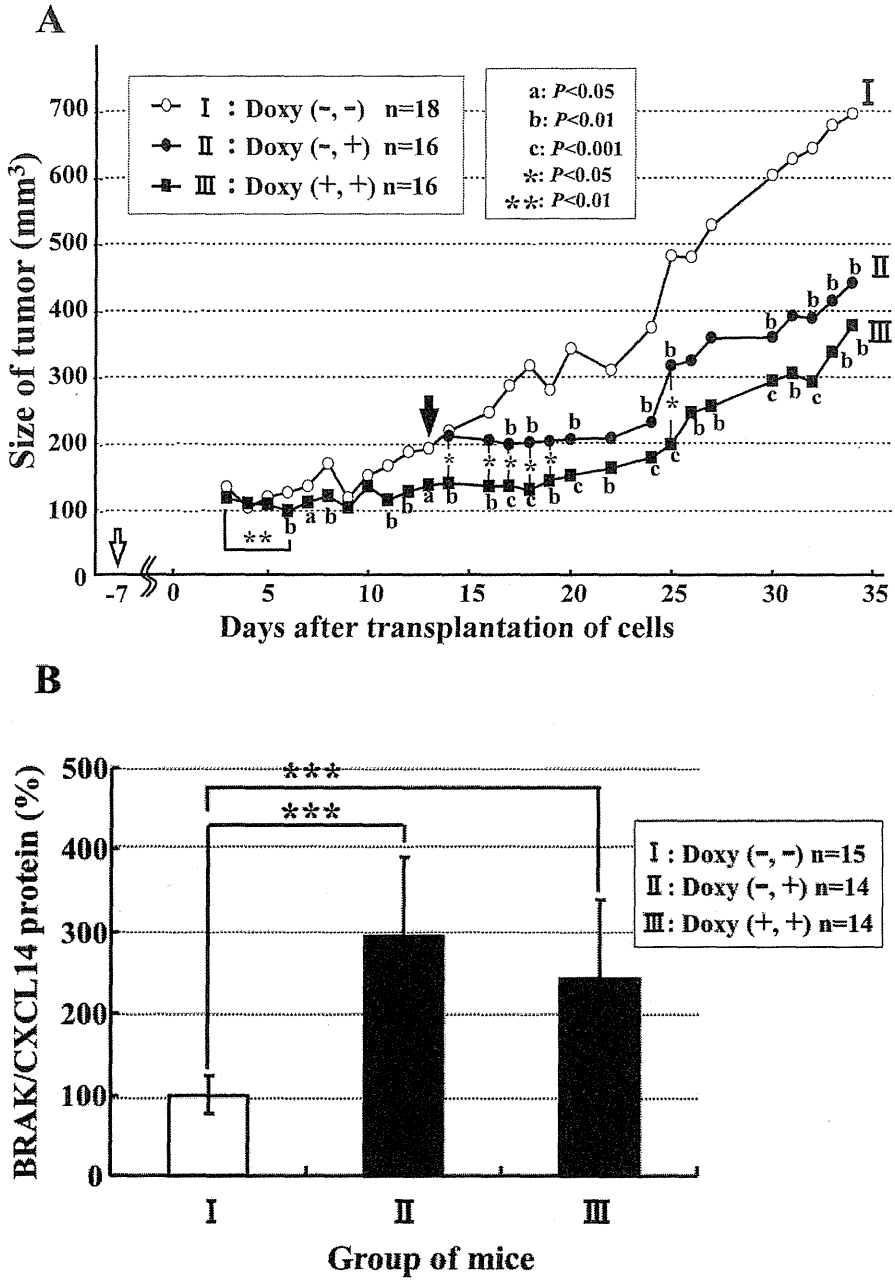

Fig. 3 Expression of BRAK/CXCL14 protein in tumor cells suppressed growth of the cells *in vivo*.
(A) Tumor size of xenografted Tet-on BRAK HSC-2 cells. The mice were subcutaneously injected with 10^7 Tet-on BRAK HSC-2 cells, and the animals were provided 5% sucrose-containing water (Group I). Other mice were given sucrose solution containing 2 mg/mL doxycycline starting at 13 days (black arrow) after implantation of the tumor cells (Group II). A third group of mice were implanted with Tet-on BRAK HSC-2 cells that had been precultured in the presence of 0.1 μg/mL of doxycycline for 7 days (Group III). These mice were provided doxycycline-supplemented water 7 days before (white arrow) implantation of the tumor cells. a, $P < 0.05$; b, $P < 0.01$; and c, $P < 0.001$ between group I and II or III. *, $P < 0.05$ between group II and III and **, $P < 0.01$ between day 3 and day 6 of group III.
(B) Expression levels of BRAK/CXCL14 proteins in transplanted tumor cells *in vivo* 35 days after transplantation, as determined by Western blotting. ***, $P < 0.001$, as indicated by the bracket.